Cold Season Cloud Response to Sea Ice Loss in the Arctic

Yinghui Liu[a] and Jeffrey R. Key[a]

[a] *Center for Satellite Applications and Research, NOAA/NESDIS, Madison, Wisconsin*

ABSTRACT: Based on satellite observations, we investigate the cloud responses during the cold season, from October to the following March, to interannual fluctuations in Arctic sea ice concentrations during September and October. It is found that the cloud responses differ between the periods 2000–18 and 1982–99. From 2000 to 2018, increased Arctic Ocean cloud cover in October and November transitioned to significantly less cloud cover and cloud radiative forcing (CRF), from January to March, in response to lower sea ice concentrations in September and October. The lower CRF from January to March preconditions the sea ice and likely contributes to higher sea ice concentrations the following September. This suggests a negative cloud feedback on sea ice concentration, which may contribute to sea ice recovery after a dramatic decrease. In contrast, from 1982 to 1999, generally increased cloud cover and cloud radiative forcing persisted from October to March following lower sea ice concentrations in the preceding September and October. The cause of the different cloud responses to sea ice changes in these two time periods remains unclear and requires further investigation.

KEYWORDS: Arctic; Feedback; Cloud radiative effects; Clouds; Ice loss/growth

1. Introduction

Clouds play a crucial role in the climate system, responding to climate change and providing feedback to the global climate. Our understanding of cloud processes and feedback has significantly advanced, leading to a reduction of approximately 50% in the uncertainty associated with cloud feedback since the Fifth Assessment Report of the United Nations Intergovernmental Panel on Climate Change (IPCC). However, in the Sixth Assessment Report of the IPCC, clouds still contribute the largest share of overall climate feedback uncertainty (Arias et al. 2023). To achieve a better understanding of cloud processes and feedbacks, continuous observation of cloud properties and improvements in cloud models are necessary. In the polar regions, the harsh and unique environment presents challenges for observing cloud properties through in situ and satellite platforms, as well as for understanding cloud formation, maintenance, and dissipation mechanisms. It is imperative to make further efforts to enhance our understanding of cloud feedbacks in the polar regions (Arias et al. 2023; Tan and Storelvmo 2019).

One intriguing area of research in understanding Arctic cloud processes is the interaction between clouds and sea ice, particularly with the substantial changes in Arctic sea ice in recent decades. Since the advent of satellite records in the early 1980s, Arctic sea ice has exhibited a decline in areal extent throughout the year, a reduction in thickness, and a shift from multiyear sea ice to first-year sea ice (Meier and Stroeve 2022; Liu et al. 2020; Kwok 2018). Notably, the most pronounced changes in sea ice concentration occur in the Beaufort, Chukchi, East Siberian, and Laptev Seas during September and October (Meier and Stroeve 2022). It has been shown that changes in sea ice during September and October have an impact on cloud properties. For instance, larger cloud amounts are observed due to stronger surface evaporation, warmer surface temperatures, and changes in the lower-tropospheric structure (Palm et al. 2010; Kay and Gettelman 2009; Taylor et al. 2015; Schweiger et al. 2008; Liu et al. 2012a). On a seasonal time scale, anomalous cloud amounts and cloud radiative forcing (CRF) from January to March over the Arctic Ocean influence sea ice growth and precondition the extent of sea ice the following summer (Liu and Key 2014; Letterly et al. 2016; Wang et al. 2019). Additionally, CRF in late spring and summer impacts sea ice extent during the summer and fall (Huang et al. 2021; Kapsch et al. 2013). This connection can be attributed to thicker (thinner) sea ice melting slower (faster) due to negative CRF at the surface, and ice motion can transport ice to other parts of the Arctic Ocean.

Despite the pronounced overall decline, sea ice concentration exhibits strong interannual and decadal variations (Meier and Stroeve 2022). Recent studies have demonstrated that sea ice changes in September and October result in atmospheric responses in the subsequent months (Simon et al. 2020; Ding et al. 2021). However, the cloud responses in the months following sea ice variations in September and October were not investigated in those studies. Decrease in cloud amount in wintertime, along with an associated negative CRF, facilitates sea ice growth, resulting in a thicker sea ice cover in the winter and leading to a slower sea ice melt and a larger sea ice extent in the subsequent summer and fall. Liu and Key (2014) and Letterly et al. (2016) demonstrated the latter feedback, where a decrease in wintertime cloud amount can lead to an increase in summertime ice concentration/extent. However, changes in wintertime cloud amount in the months

---

Key's current affiliation: Cooperative Institute for Meteorological Satellite Studies, University of Wisconsin–Madison, Madison, Wisconsin.

Corresponding author: Yinghui Liu, yinghui.liu@noaa.gov

following sea ice loss in September and October have not previously been investigated. Here, we examine wintertime cloud amount changes related to sea ice conditions the previous summer.

2. Data and method

a. Data

This study utilizes monthly means of sea ice concentration (SIC), cloud amount and CRF at the surface, geopotential height, and wind in the Arctic, along with global sea surface temperature (SST) and snow-cover data, covering the period from 1982 to 2018. CRF is a measure of the cloud's impact at the surface or top of the atmosphere (TOA) and is defined as the difference between the all-sky and clear-sky net radiation fluxes at the surface or TOA. Monthly mean SIC data were obtained from the Climate Data Record (CDR) of sea ice concentration based on passive microwave data (Meier et al. 2021) at a resolution of 25 km in a polar stereographic map projection. Cloud amount and CRF are from two datasets: the extended Advanced Very High Resolution Radiometer (AVHRR) Polar Pathfinder (APP-x) CDR and the Clouds and the Earth's Radiant Energy System (CERES) Energy Balanced and Filled (CERES_EBAF) Edition 4.1 (CERES_EBAF_Edition 4.1). The APP-x monthly mean cloud amount and CRF have a spatial resolution of 25 km in the Equal-Area Scalable Earth (EASE) Grid (Key et al. 2016). The APP-x monthly means were derived from twice-daily retrievals at two local solar times in the Arctic, 0400 and 1400. The main inputs for the APP-x dataset are the AVHRR channel data (reflectances, brightness temperatures, viewing and illumination geometry, and time). APP-x applies multiple spectral and temporal tests specifically designed for cloud detection in the polar regions (Key and Wang 2015). The CERES_EBAF_Edition 4.1 monthly mean cloud amount and CRF have a 1° latitude/longitude spatial resolution. The CERES_EBAF_Edition 4.1 dataset is available for the period after 2000. It utilizes observations from CERES and Moderate Resolution Imaging Spectroradiometer (MODIS) (Trepte et al. 2019). CERES uses multiple spectral tests with MODIS data in cloud detection (Kato et al. 2020).

Monthly mean SSTs were obtained from the Extended Reconstructed Sea Surface Temperature (ERSST) dataset (Huang et al. 2020). The ERSST is derived from the International Comprehensive Ocean–Atmosphere Data Set (ICOADS) (Huang et al. 2020). The Pacific decadal oscillation (PDO) characterizes a long-lived El Niño–like pattern of Pacific climate variability (Mantua et al. 1997; Newman et al. 2016). The National Centers for Environmental Information (NCEI) PDO index, which is based on ERSST and closely follows the Mantua PDO index (Mantua and Hare 2002), was used in this study. Monthly mean winds, temperature, and geopotential heights at 1000, 925, 850, 700, and 500 hPa are from the dataset of fifth major global reanalysis produced by ECMWF (ERA5) (Hersbach et al. 2020). Monthly snow amounts were derived from the Rutgers Northern Hemisphere 24-km weekly snow-cover extent (Robinson and Estilow 2021) obtained from the National Snow and Ice Data Center (NSIDC, Boulder, Colorado).

b. Method

To remove long-term trends in the monthly means of SIC, cloud amount, CRF, SST, and snow cover, a quadratic polynomial fit to each was subtracted. This process retained the interannual variations, with some decadal and longer fluctuations still present (Simon et al. 2020). Ding et al. (2021) demonstrated that the SIC variability in September from 1979 to 2018 exhibited high correlations with the SIC variability in October, and neither had an apparent connection with the SIC variations in November and December. They also showed that the September–October (SO) mean SIC could effectively represent the interannual variation of Arctic sea ice in autumn and be used to investigate its impact on the winter climate variability. Furthermore, they found that the first two empirical orthogonal function (EOF) modes of the SO SIC time series captured the interannual variability of SIC in the East Siberian–Chukchi–Beaufort Seas (EsCB) and the Barents–Kara–Laptev Seas (BKL) (Fig. 1).

In this study, a similar approach was adopted to define the leading interannual variations of SIC. The time series of the area-mean SO SIC anomalies in the regions 70.5°–82.5°N, 135.5°E–119.5°W, and 70.5°–80.5°N, 40.5°–134.5°E were normalized by their standard deviations, were multiplied by −1, and were used as indices to represent the SIC variations in the EsCB and BKL, respectively (Fig. 2). A negative sea ice anomaly is a positive sea ice index, and vice versa. A distinction between this study and Ding et al. (2021) lies in the preprocessing of the SIC time series. Here, the removal of the quadratic polynomial fit was employed as in Simon et al. (2020) and Fučkar et al. (2016), whereas Ding et al. (2021) used a 9-yr high-pass filter. Detrending with a third-order polynomial fit and a linear trend generates very similar sea ice indices as those with a quadratic fit (Fig. 1) and do not change the main conclusions of this study.

The cloud responses, including cloud amount and CRF, to the interannual SIC variations were determined by calculating lag correlations and lag regressions of atmospheric parameter means in October–November (ON), November–January (NDJ), and January–March (JFM) with the SO SICs, where the lag periods were 1, 2, and 4 months, respectively. Additionally, simultaneous correlations and regressions of SST and snow cover with the SICs in SO were calculated to account for other forcings that may influence the atmospheric response. This consideration is necessary because it is possible that SIC, SST, and snow cover are influenced by the same forcing factor (Simon et al. 2020). The correlations/regressions were calculated by correlating the sea ice indices and detrended variables at each grid cell. All the variables in the data section were detrended with a quadratic polynomial fit before the correlation/regression calculations. The statistical significance of the lag and simultaneous correlations/regressions were evaluated using a two-tailed Student's t test at the 95% confidence level. Because the focus of this study is the winter cloud response to sea ice conditions the previous summer and its possible impacts on the sea ice conditions the following summer, only the cloud response over the sea ice–covered areas is considered, excluding Greenland Sea. Auxiliary figures of this study can be found in the appendix.
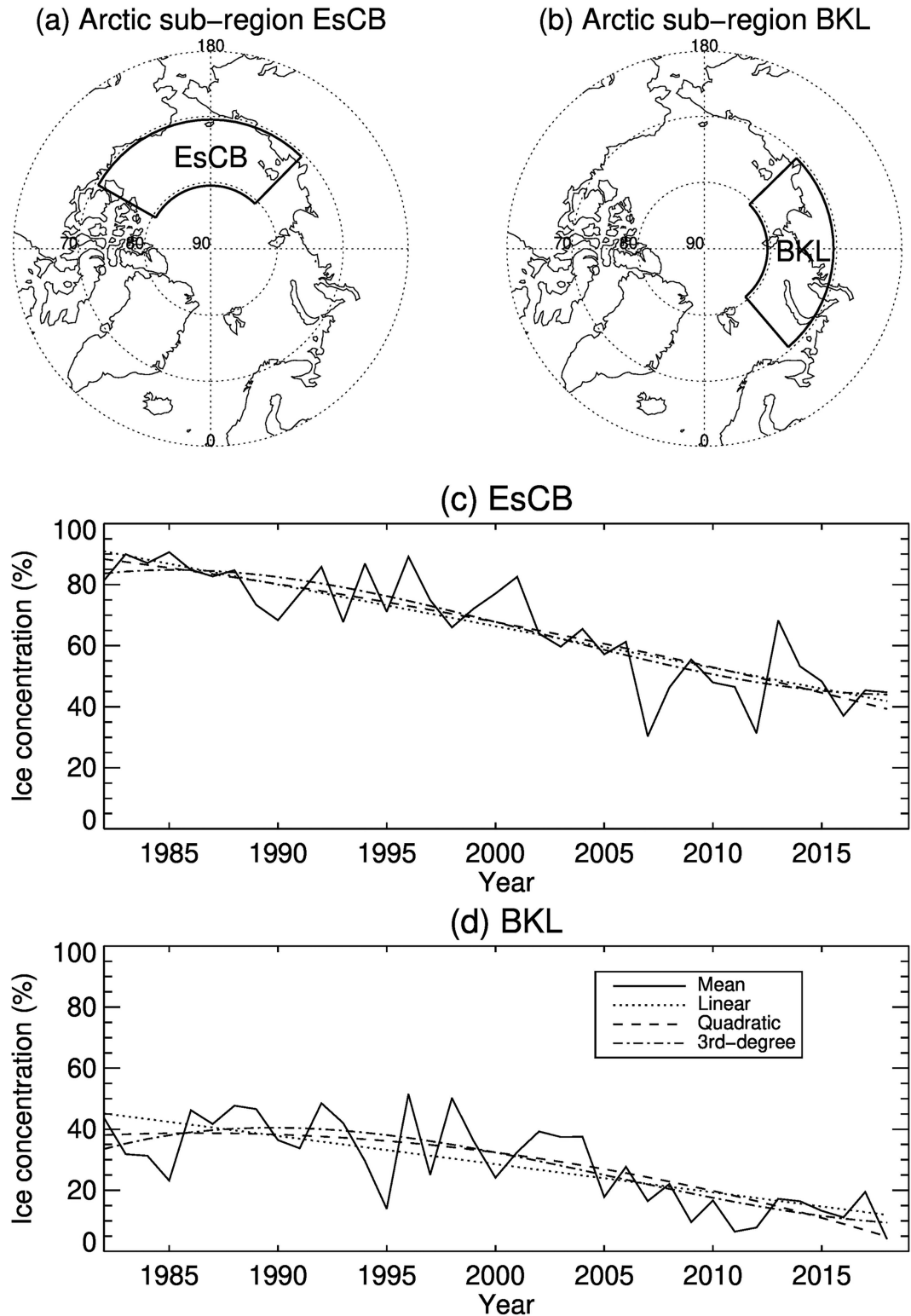
FIG. 1. Locations of (a) EsCB and (b) BKL and time series of mean SICs and linear, quadratic, and third-degree polynomial fit over (c) EsCB and (d) BKL.
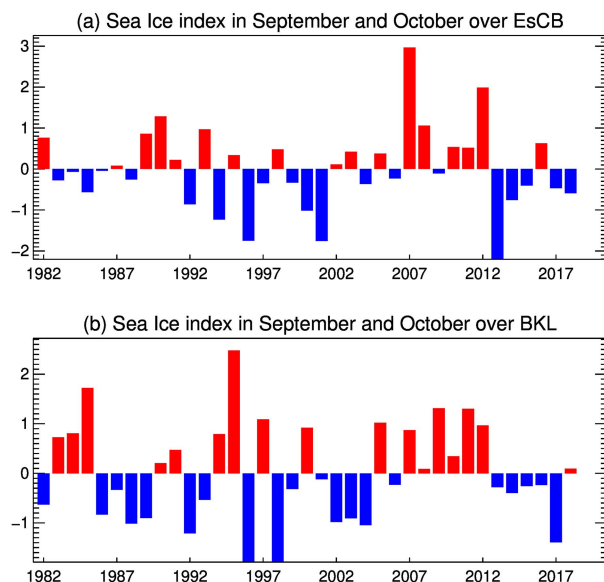
FIG. 2. Sea ice index (SIC anomalies for SO multiplied by −1) over the EsCB and the BKL from 1982 to 2018.

Collections of multiple statistically significant tests at numerous spatial grid points do not necessarily confirm the global null hypothesis (Livezey and Chen 1983). To assess field significance, the collective significance of individual tests at these grid points needs to be considered (Livezey and Chen 1983; Wilks 2016). One method to evaluate field significance is based on the concept of the false discovery rate (Wilks 2016; Renard et al. 2008). This involves determining a false discovery rate probability from all *p* values of the individual tests across the spatial grid points. Field significance is declared if at least one grid point has a *p* value smaller than this probability (Renard et al. 2008). Detailed explanations of this approach are available in Wilks (2016), Renard et al. (2008), and their cited references. In this study, field significance tests (FSTs) were conducted based on individual tests over the sea ice–covered Arctic Ocean to assess the overall significance between sea ice indices and changes in cloud amount and CRFs. The grid points with *p* values smaller than the false discovery rate probability are indicated in the figures.

3. Results

The CERES_EBAF_Edition 4.1 dataset is available starting from the year 2000, while the APP-x dataset covers the period from 1982. However, in this study, the APP-x data after 2018 were not included due to the orbital drift of the NOAA-19 satellite Equatorial Crossing Time, which resulted in larger uncertainties in the monthly means after 2018. Therefore, the analysis focused on the period from 2000 to 2018 to ensure consistency and also cross validation of the findings using both datasets. The results of this analysis are presented in section 3a. To further confirm the findings using data from 2000 to 2018, a separate analysis was conducted using only the APP-x dataset for the period from 1982 to 1999. This additional analysis is described in section 3b.

Both time periods, 1982–99 and 2000–18, have similar durations of 18 years and 19 years, respectively.

a. Cloud response to SO SIC 2000–18

The analysis of the APP-x cloud amount in relation to the SO SIC index over the EsCB yields several findings. First, the decrease in SO SIC over EsCB is associated with a general increase in cloud amount during ON, a general decrease in cloud amount during NDJ, and a significant decrease—both significant with individual significance tests at grids and field significance test—in cloud amount during JFM over the Arctic Ocean (Fig. 3). The lag correlation and regression coefficients between the ON cloud amount and SO SIC index show positive values locally over EsCB, although they are not statistically significant. This positive correlation is consistent with previous findings that the presence of newly open water over the Arctic Ocean leads to increased cloud amount due to enhanced surface evaporation. In NDJ, the cloud amount exhibits a negative relationship with the SO SIC index over the Arctic Ocean, except for a limited area in the Kara Sea. (Note that a negative sea ice anomaly in SO is a positive sea ice index as defined here.) The negative relationship becomes significant during JFM, indicating that the decreased SIC over EsCB in SO is followed by a significant decrease in cloud amount over the Arctic Ocean in JFM.

The lag correlation and regression of the cloud amount on the SO SIC index over the BKL suggest that the SO SIC decrease over BKL is followed by a general, albeit weak, decrease in cloud amount, except for the BKL region itself, during ON. In NDJ, a decrease in cloud amount is observed over parts of the Arctic Ocean. This decrease becomes even more pronounced and significant during JFM—both significant with individual significance tests at grids and field significance test—covering most of the Arctic Ocean (Fig. 4). In the BKL region, the relationships between cloud amount and SO SIC index are positive, indicating a strong local impact of increased surface evaporation. The magnitude of the cloud amount decrease associated with one standard deviation of SIC is over 4.0% over the Arctic Ocean for EsCB and over 6.0% over the Arctic Ocean for BKL, indicating a stronger influence from the BKL region.

Arctic clouds generally have a warming effect on the surface throughout most of the year, except during a short period in summer. While cloud amount is an important factor, the impact of Arctic clouds on radiative fluxes at the surface and TOA is influenced by various factors, including cloud properties, solar zenith angle, surface albedo, and other variables (Intrieri et al. 2002; Shupe and Intrieri 2004). Because downward longwave radiation at the surface increases with cloud coverage, it is generally expected that larger cloud amounts result in radiative warming at the surface in the Arctic and lower cloud amounts result in radiative cooling, particularly during the period from January to March (Intrieri et al. 2002). The lag correlation and lag regression analysis of the APP-x CRF on the SO SIC index over EsCB and BKL supports this expectation (Figs. 5 and 6). The results demonstrate that a decrease in the SO SIC over EsCB and BKL is followed by a
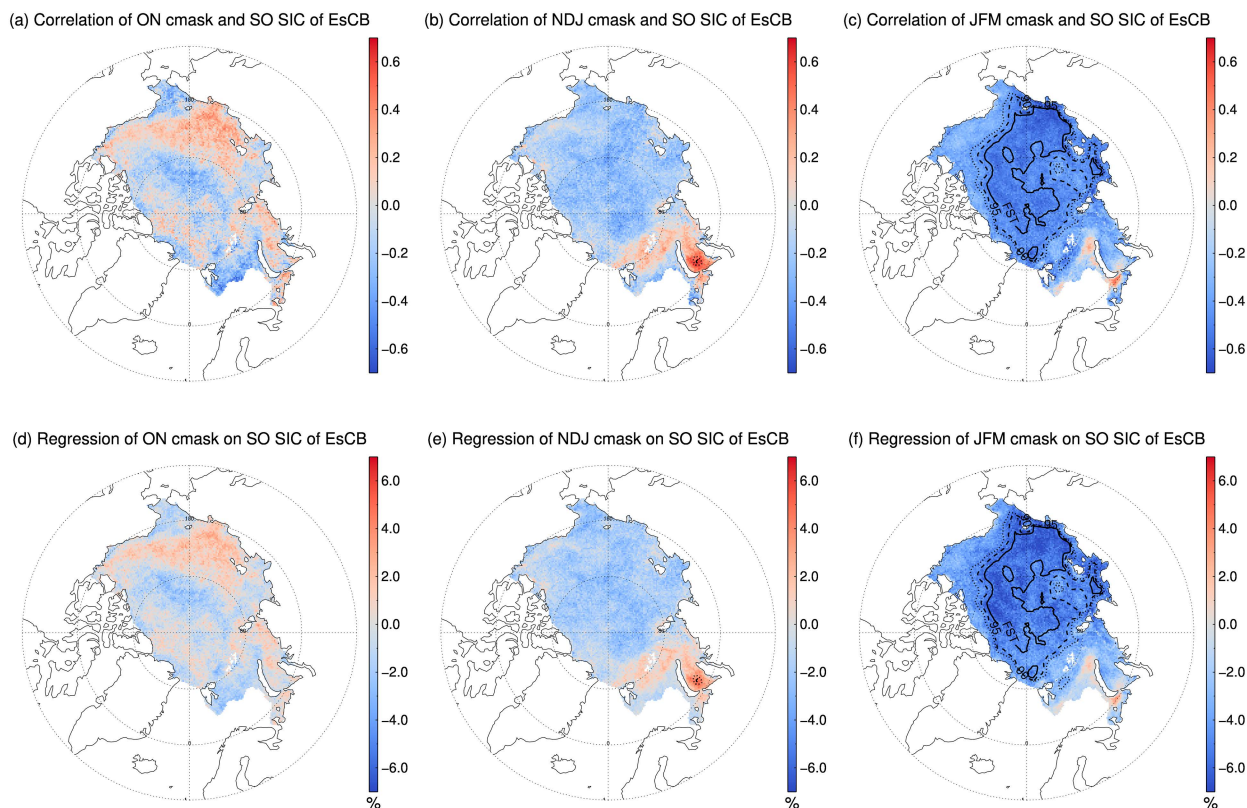
FIG. 3. Correlations of the APP-x cloud amounts (cmask) in (a) ON, (b) NDJ, and (c) JFM with sea ice index in SO for the period 2000–18 over the EsCB. The lag regression coefficients of the cloud amounts (cmask) on the SO sea ice index over EsCB for 2000–18 are in (d) ON, (e) NDJ, and (f) JFM. The dotted-line and dashed-line contours denote that correlations/regressions with higher than 90% and 95% confidence levels, respectively. The solid-line contours denote the areas with p values smaller than the false discovery rate probability, meaning that they pass the FST.

combination of positive and negative CRF during ON, negative CRF (cooling) during NDJ, and significantly negative CRF during JFM over the Arctic Ocean. The magnitude of this decrease is estimated to be approximately 3.0 W m^{-2} for a one standard deviation decrease in SIC over EsCB and 4.0 W m^{-2} over BKL from January to March. It should be noted that the correlations between JFM CFRs and SO SIC index pass the field significance test for BKL but not for EsCB. While there are noticeable differences between the spatial patterns shown in Figs. 3 and 4, the overall lag correlation/regression patterns are similar. These differences might be attributed to additional factors that influence cloud radiative forcing, such as changes in cloud properties resulting from SIC variations, which were not included in this study.

The lag correlation and lag regression analysis of the CERES_EBAF_Edition 4.1 cloud amount on the SO SIC index over EsCB and BKL reveals similar patterns to those observed with the APP-x dataset. Specifically, there is a general increase in cloud amount during ON, particularly over EsCB, and a decrease in cloud amount during JFM over the Arctic Ocean (Fig. A1) after an anomalously low SO ice concentration. However, the correlations between JFM cloud amount anomalies and SO SIC indices do not pass the field significance test, though individual significance tests show statistical

significance. The significant decrease in cloud amount during JFM, as indicated by CERES, appears to be weaker and less extensive over the Arctic Ocean compared to the results from APP-x. For example, a one standard deviation decrease in SIC over EsCB leads to a cloud amount decrease of over 3.0% mainly over areas north of the Canadian Archipelago and East Siberian Sea based on CERES, whereas the APP-x dataset shows a 4.0% cloud amount decrease over most of the Arctic Ocean. Similarly, a one standard deviation decrease in SIC over BKL leads to a cloud amount decrease of over 3.0% over areas extending from north of Greenland to the East Siberian Sea based on CERES, while the APP-x dataset exhibits a stronger decrease of over 6.0% over the Arctic Ocean. Despite these differences in magnitude and spatial extent, both datasets suggest a decrease in cloud amounts during JFM over the Arctic Ocean following the decrease in SO SIC. Furthermore, a negative correlation and regression are found between the CERES cloud radiative forcing (CRF) in JFM and the SO SIC over EsCB, which is consistent with the findings for CERES cloud amount and those based on APP-x in Fig. 4. However, no significant negative correlation and regression are found between the CERES CRF in JFM and the SO SIC over BKL, even though such a negative correlation/regression exists for cloud amounts.

(a) Correlation of ON cmask and SO SIC of BKL

(b) Correlation of NDJ cmask and SO SIC of BKL

(c) Correlation of JFM cmask and SO SIC of BKL

(d) Regression of ON cmask on SO SIC of BKL

(e) Regression of NDJ cmask on SO SIC of BKL

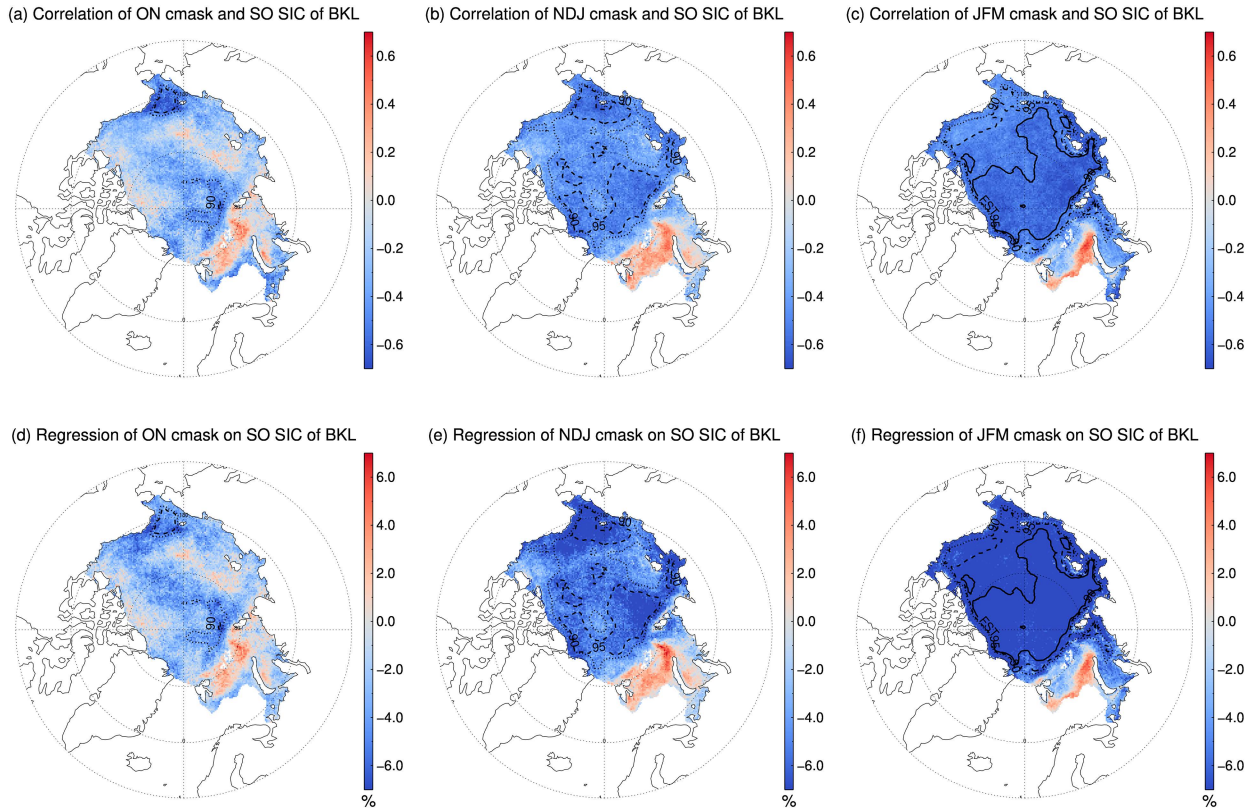(f) Regression of JFM cmask on SO SIC of BKL

FIG. 4. As in Fig. 3, but for the sea ice index over the BKL.

The anomalous cloud amount and CRF in JFM following changes in the SO SIC over the EsCB and BKL have implications for sea ice growth in winter and preconditioning of the sea ice over the Arctic Ocean in the subsequent summer and fall. The negative surface radiation flux anomalies over the Arctic Ocean in January–February 2013, resulting from below average cloud amount, cooled the surface and facilitated greater ice growth. This phenomenon played a role in the recovery of sea ice extent in September 2013 following the satellite-record low ice extent observed in September 2012 (Liu and Key 2014). Studies have demonstrated that cloud-forcing anomalies in the East Siberian and Kara Seas during winter can precondition the sea ice and explain 25% of the September sea ice concentration variations (Letterly et al. 2016). A similar mechanism has been observed in Antarctica, where negative cloud-fraction anomalies during winter 2011 contributed to the positive Antarctic sea ice anomaly in summer 2012 (Wang et al. 2019).

Following the approach in Liu and Key (2014), and similar to those in other studies (Thorndike 1992; Eisenman et al. 2007), the relationship between surface radiation and a change in ice thickness can be presented as

$$\Delta h = \frac{t}{\rho L}(F_{\text{srf\_net\_clear}} + F_{\text{srf\_CRF}}),$$

where Δh is the change in ice thickness, t is the length of the time period, ρ is the density of sea ice, L is the latent heat of

fusion for sea ice, $F_{\text{srf\_net\_clear}}$ is the surface net radiation for clear sky, and $F_{\text{srf\_CRF}}$ is the surface net CRF. Surface sensible heat and surface latent heat are neglected because they are much smaller than the radiative fluxes. With this simple method, 1 W m^{-2} of negative monthly net cloud radiative forcing anomaly would grow 0.85 cm of sea ice.

The CRF changes over the Arctic Ocean in JFM of a particular year, resulting from the SO SIC changes in the previous year, can be calculated by multiplying the regression coefficients between the CRF in JFM (Figs. 5f and 6f) and the SO SIC index over the EsCB and BKL (Fig. 2). In the case of an anomalous year such as 2013, when a satellite-recorded low sea ice extent occurred in 2012, the SIC index over EsCB is close to 2, and over BKL, it is close to 1. The derived CRF in JFM for 2013 is around -10 W m^{-2} on a monthly scale over most of the Arctic Ocean (Fig. 7a). The negative CRF contributes to greater sea ice growth, and by the end of March 2013, the sea ice thickness anomaly reaches approximately 30 cm (Fig. 7b). In contrast, in 2002, when the sea ice index is negative over both EsCB and BKL, the derived CRF in JFM for 2002 is approximately 5 W m^{-2} on a monthly scale over most of the Arctic Ocean (Fig. 8a). The positive CRF results in less sea ice growth, and by the end of March 2002, the sea ice thickness anomaly is close to -15 cm (Fig. 8b).

To illustrate the effects of these anomalous sea ice growth patterns in winter on the late summer sea ice field, sea ice motion vectors from the Polar Pathfinder daily, 25-km EASE
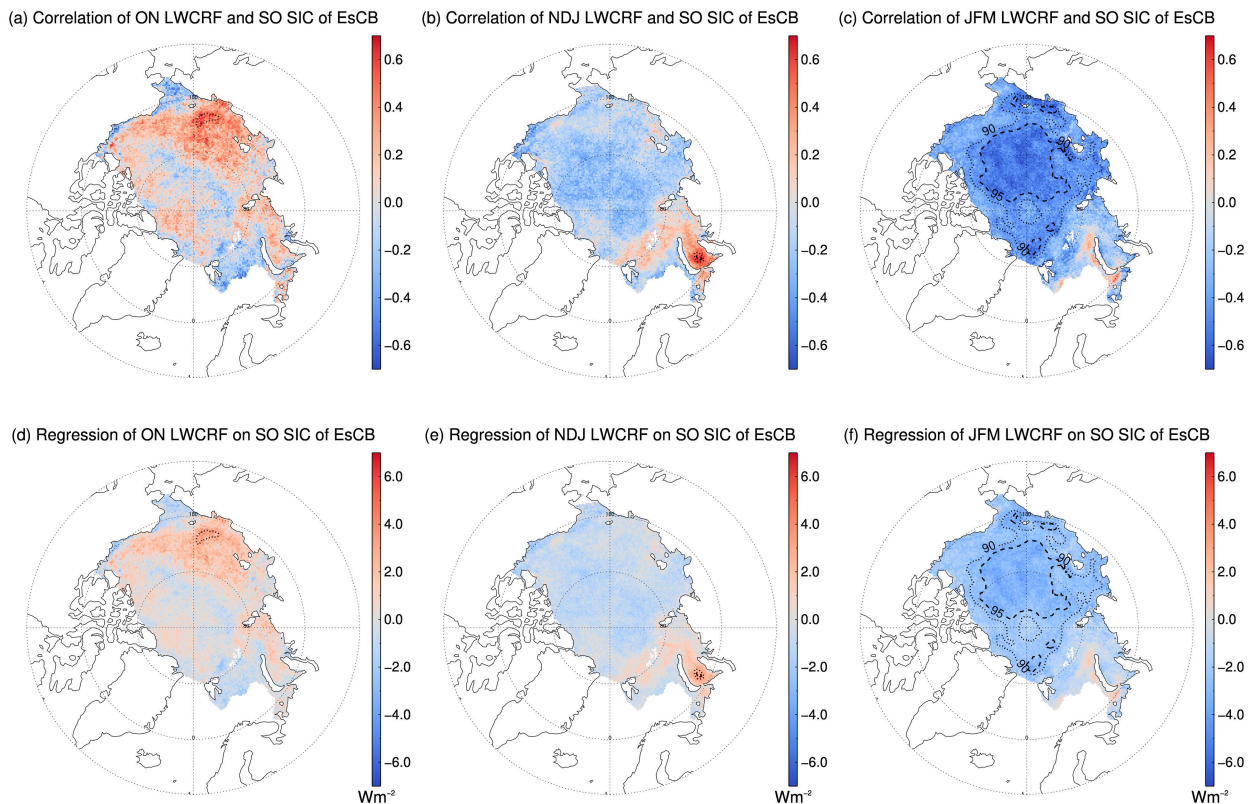
FIG. 5. As in Fig. 3 (EsCB region), but for Longwave Cloud Radiative Forcing (LWCRF) instead of the cloud amount.

Grid products (Tschudi et al. 2020) are used to drive the initial sea ice growth anomaly field from 31 March (Figs. 7b and 8b) until 1 September. These simulations assume no other factors affecting the sea ice. As a result, a negative sea ice thickness anomaly would be expected over the Arctic Ocean in September 2002 and a positive sea ice thickness anomaly would be expected in September 2013. These anomalies contribute to the sea ice return observed in late summer 2013, as shown in Liu and Key (2014).

b. Cloud response to SO SIC 1982–99

The lag correlation and lag regression analysis of the APP-x cloud amount on the SO SIC index over the EsCB and BKL for the time period from 1982 to 1999 shows different features compared to the analysis conducted for the period from 2000 to 2018. For the SO SIC decrease over EsCB, the analysis indicates a general mixed pattern of increased and decreased cloud amount in ON, a general increased cloud amount in NDJ, and increased cloud amount in JFM over the Arctic Ocean (Fig. 9). However, these correlations and regressions are not statistically significant. The results in NDJ and JFM differ from those obtained using data from 2000 to 2018. Similarly, for the SO SIC decrease over BKL, the analysis reveals a general mixed pattern of increased and decreased cloud amount in ON, NDJ, and JFM over the Arctic Ocean (Fig. 10), and these correlations and regressions are not statistically significant.

c. Differences between 1982–99 and 2000–18

The relationship between the SO SIC index over EsCB and the cloud amount in NDJ and JFM over the Arctic Ocean shows opposite patterns between the time periods of 1982–99 and 2000–18. For the period of 1982–99, the relationship is positive, indicating that higher SO SIC index values over EsCB are associated with increased cloud amounts in NDJ and JFM over the Arctic Ocean. This positive correlation is observed in a wider area. However, for the period of 2000–18, the relationship has switched to negative. This means that higher SO SIC index values over EsCB are now associated with decreased cloud amounts in NDJ and JFM over the Arctic Ocean. The negative correlations observed during this period are statistically significant with individual significance tests and the field significance test. The time series analysis of the SO SIC index over EsCB and the cloud amount anomaly over a randomly selected location within the area between 150° and 240° longitude and latitude 70°–85°N latitude (Fig. 11) further illustrates this opposite trend. After 2000, particularly in 2001, 2007, and 2012, the SO SIC index and cloud amount anomaly in JFM show opposite variations. It is worth noting that 2007 and 2012 were years with record-low Arctic sea ice extents, while the sea ice extent in 2001 was above the September average. Additionally, when the data from 1 year after 2000 with a high SO SIC index, such as 2007 or 2012, are removed from the time series, the negative correlation/regression between JFM clouds and the SO index remains
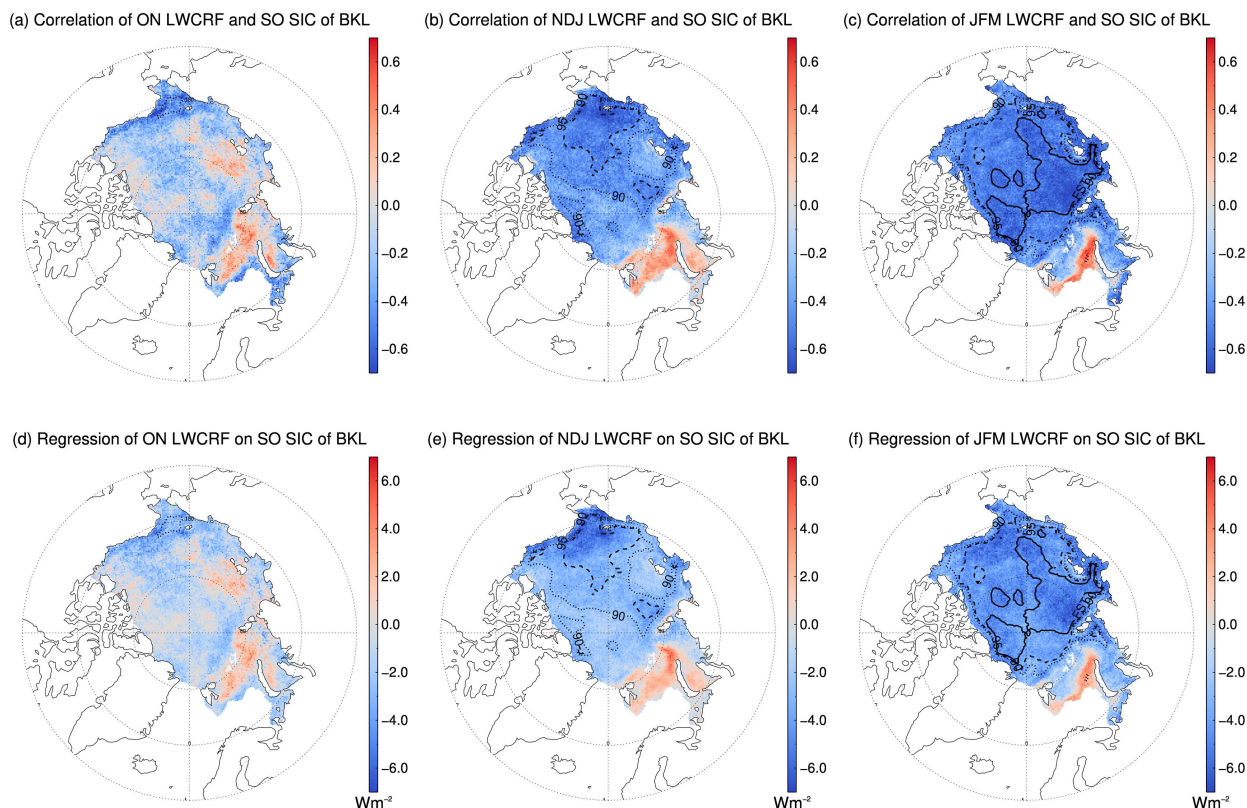
FIG. 6. As in Fig. 4, but for LWCRF over BKL region.

statistically significant over the Arctic Ocean, as depicted in Figs. 3 and 4.

Though cloud formation and dissipation mechanisms in the Arctic are not well understood (Curry et al. 1996), a few factors are associated with cloud formation in the Arctic. These factors include, but are not limited to, moisture flux convergence, surface evaporation, and cloud microphysical processes (Beesley and Moritz 1999; Liu et al. 2007). Changes in these factors between 2000–18 and 1982–99 may lead to changes in the winter cloud responses to the sea ice variations.

The circulation in the Arctic from January to March is dominated by Icelandic Low off the southeast coast of Greenland, the Aleutian low in the North Pacific basin, and the Siberian High over east-central Asia (Serreze and Barry 2005). The circulation patterns in the Arctic during January–March play a significant role in influencing the climate conditions and weather patterns in the region. In 2000–18, during JFM, there is a distinct circulation pattern associated with years characterized by decreased SO SICs (high SO SIC index) over the EsCB and the BKL. This pattern is characterized by anomalously high
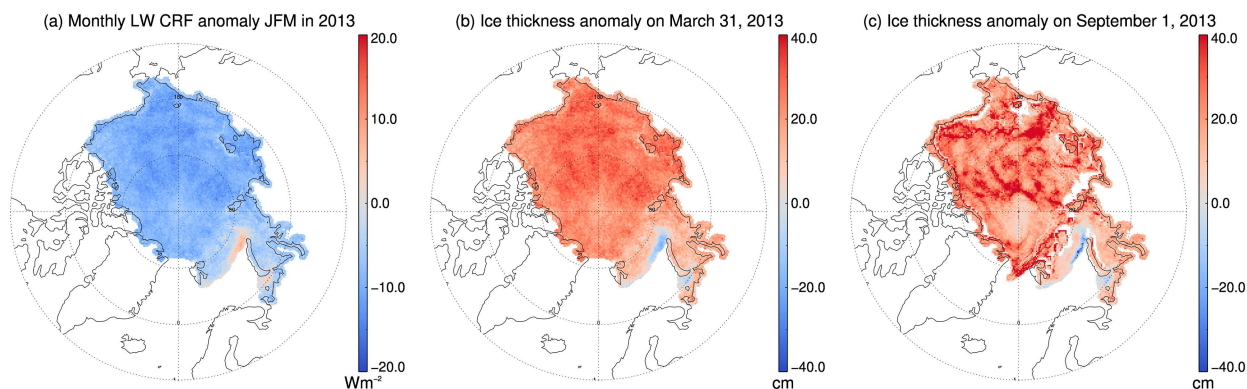

FIG. 7. (a) Monthly LWCRF anomalies in JFM in 2013 derived from the sea ice index in SO 2012; (b) anomalous sea ice growth from the anomalous LWCRF on 31 Mar 2013; and (c) possible anomalous sea ice thickness on 1 Sep 2013.
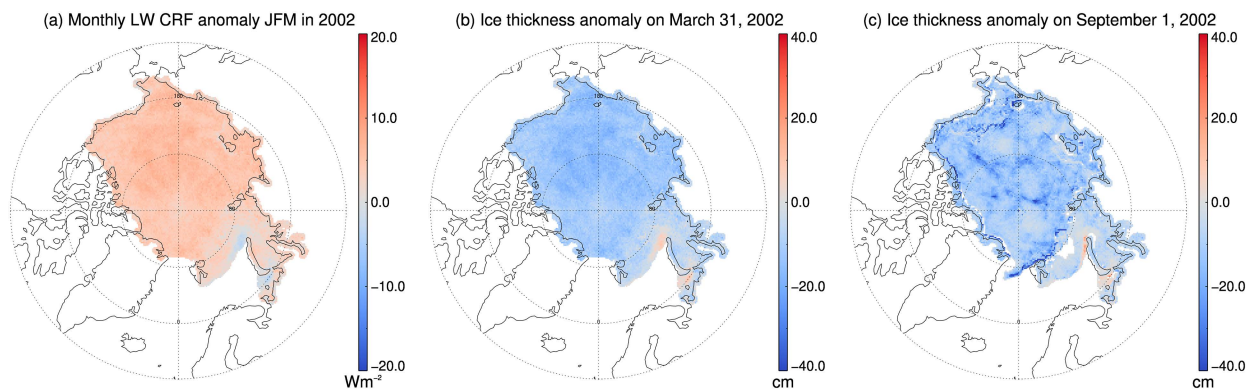
FIG. 8. As in Fig. 7, but for the 2001–02 case.

geopotential heights over the North Pacific, Greenland, and the Kara Sea, as well as east of the Kara Sea. In contrast, there are anomalously low geopotential heights over Alaska, the Bering Strait, and the North Atlantic (Fig. 12). This pattern transports cold and dry air from the continental North America over the Arctic Ocean. The opposite pattern in years with increased SO SICs (low SO SIC index) over the EsCB and the BKL favors warm air from the northeast Pacific toward Alaska and the Bering Strait and further into the Arctic Ocean due to the anomalous low pressure over the North Pacific and the anomalous high pressure over Alaska and warm air from the North

Atlantic into the Arctic Ocean due to the anomalous low pressure over Greenland. Because warmer air can hold more moisture and lead to enhanced cloud formation, these circulation anomalies create favorable conditions for lower JFM cloud amounts following years with anomalously high SO SIC index and for higher JFM cloud amounts during JFM following years with anomalously low SO SIC index.

In contrast, during the period of 1982–99, anomalously high geopotential heights occurred over the North Pacific, the eastern part of the Arctic Ocean, and anomalously low geopotential heights were observed over Canada and the North Atlantic in
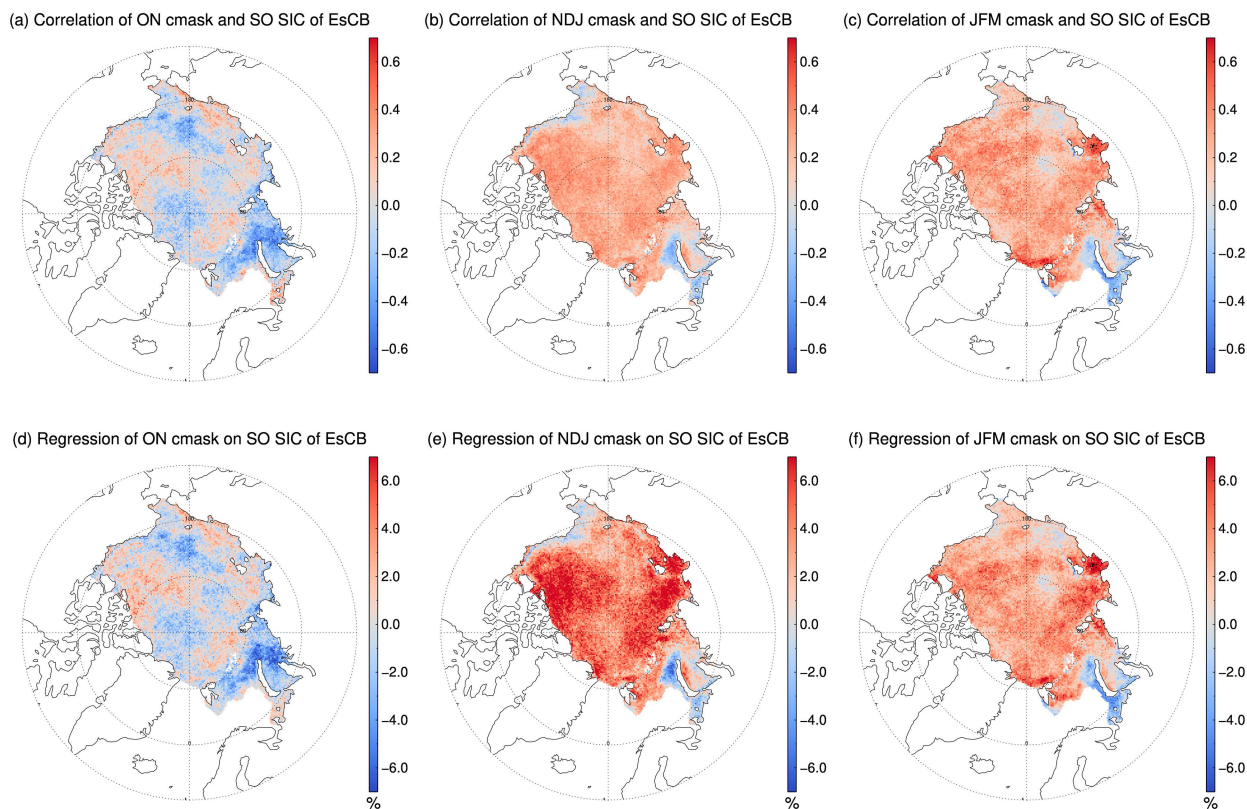

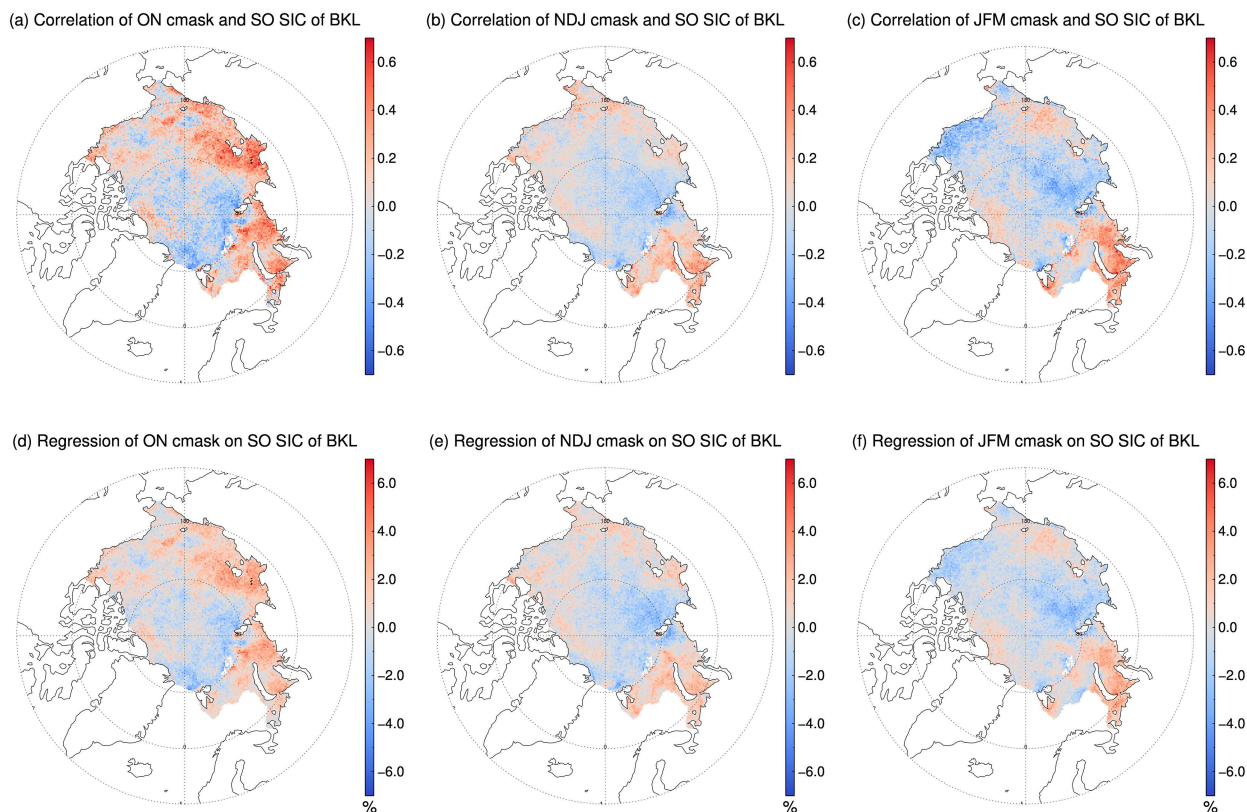FIG. 9. As in Fig. 3 (EsCB region), but for 1982–99.

FIG. 10. As in Fig. 4 (BLK region), but for 1982–99.

years characterized by decreased SO SICs (high SO SIC index) over the EsCB (Fig. 13). In this circulation pattern, there is a favorable setup for warm air from the North Atlantic Ocean to enter the Arctic Ocean through the eastern part of Greenland. As a result, during JFM, larger cloud amounts tend to appear over the Arctic Ocean following years with anomalously high SO SIC index from 1982 to 1999.
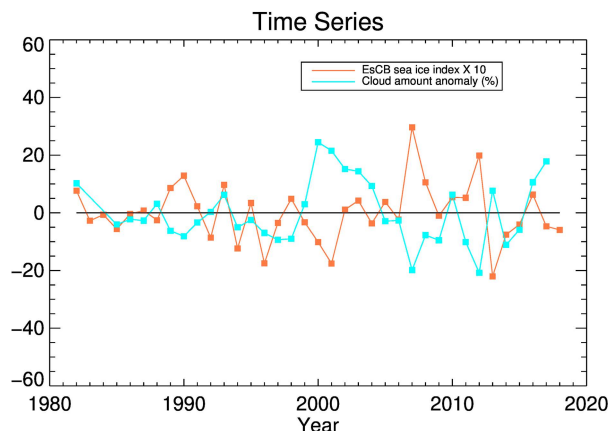

FIG. 11. Time series of the SO SIC index over the EsCB and the cloud amount anomaly over a representative location between 150°–240° longitude and 70°–85°N latitude.

Ding et al. (2021) demonstrated that the variability in SIC during September and October from 1979 to 2018 did not show a noticeable connection with SIC variations in November and December. The analysis presented here, based on the sea ice concentration CDR, showed that there were no significant correlations between the SIC of NDJ and JFM with the SO SIC index (as shown in Figs. A2 and A3, with figures for EsCB not displayed) except for limited local areas over BKL and EsCB. This finding aligns with the results of Ding et al. (2021). This indicated that anomalously low SIC in SO over the EsCB and BKL did not persist into NDJ or JFM for both 2000–18 and 1982–99 periods and did not lead to noticeable changes in surface evaporation, which neither favors nor suppresses cloud formation (Li et al. 2020). Therefore, the JFM cloud response to SO sea ice changes is unlikely to be due to changes in surface evaporation.

Beesley and Moritz (1999) suggest that temperature dependence of ice-phase microphysical processes dominates the seasonal variations in low-level cloud amount in the Arctic by affecting the condensate distribution between ice and liquid and the shorter residence time for ice particles, thus a warmer Arctic climate might lead to a longer summertime cloudy season (higher cloud amount) and a shorter winter cloudy season (lower cloud amount). Anomalously low SIC in SO over the EsCB is correlated with lower air temperature at 850 hPa over the Arctic Ocean, significant over the Pacific side of the Arctic Ocean, from 2000 to 2018 (Fig. A4), which could possibly

(a) Anomalies of geopotential height and wind in JFM at 850 hPa 2000-2018 over EsCB

(b) Anomalies of geopotential height and wind in JFM at 850 hPa 2000-2018 over BKL
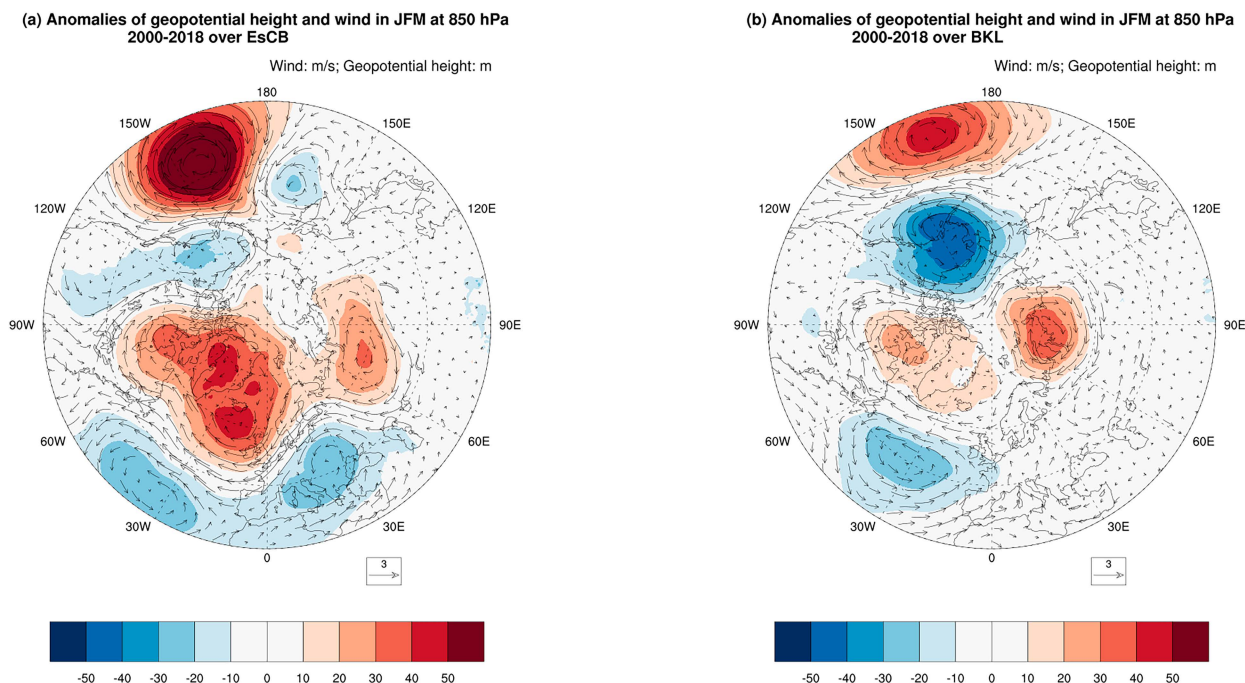

FIG. 12. Composite map of geopotential height and winds of difference between low and high SIC years over (a) the EsCB (low years: 2007, 2008, and 2012; high years: 2000, 2001, 2013, and 2014) and (b) the BKL (low years: 2000, 2005, 2007, 2009, 2011, and 2012; high years: 2002, 2003, 2004, and 2017).

contribute to the lower cloud amount. From 1982 to 1999, anomalously low SIC in SO over the EsCB is correlated with higher air temperature at 850 hPa over the Arctic Ocean (Fig. A5), which possibly contributes to the higher cloud amount. Generally,

similar relationships are also found with air temperature and SO sea ice concentration anomalies over BKL (figures not shown). However, the mechanism by which the SO SIC potentially influences the JFM 850-hPa temperature is not clear.
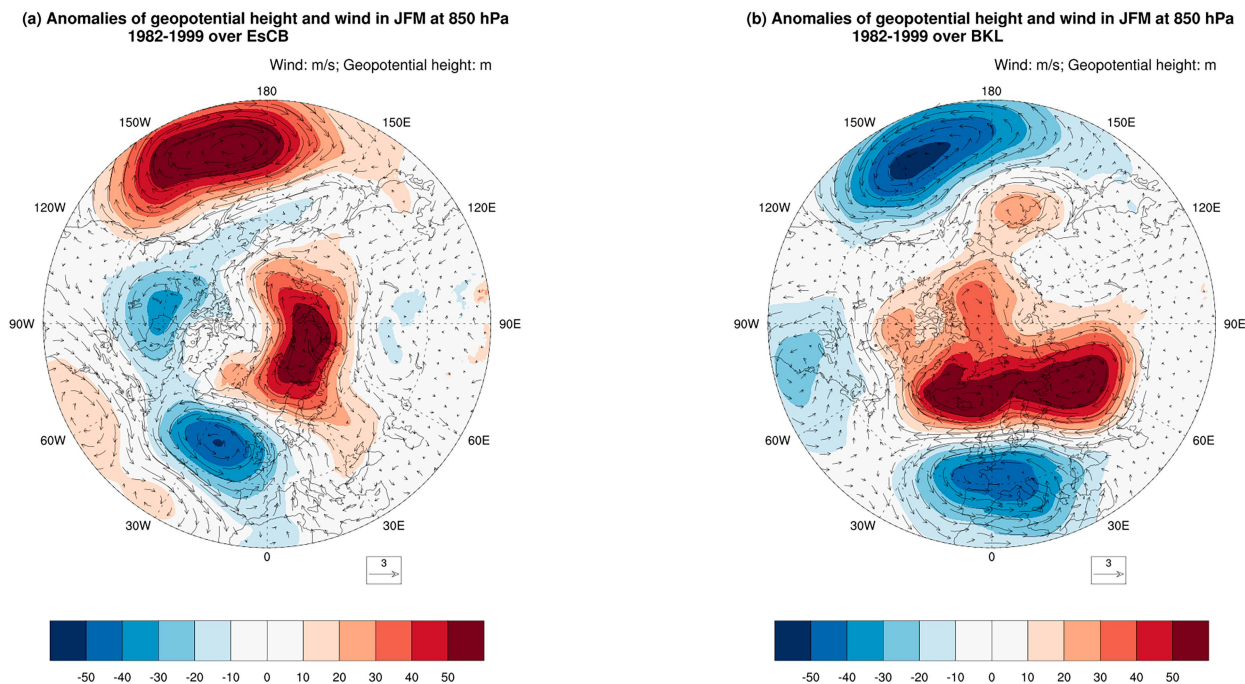
(a) Anomalies of geopotential height and wind in JFM at 850 hPa 1982-1999 over EsCB

(b) Anomalies of geopotential height and wind in JFM at 850 hPa 1982-1999 over BKL

FIG. 13. As in Fig. 12, but for 1982–1999.

4. Discussion

An analysis of the APP-x dataset for two different time periods, 1982–99 and 2000–18, was performed. Results indicate that during the period 2000–18, anomalously low SO SICs over the EsCB and BKL precede significantly fewer clouds and lower CRF over the Arctic Ocean during JFM. However, during the period from 1992 to 1999, the opposite occurs, where anomalously low SO SICs over EsCB precede more clouds and higher CRF over the Arctic Ocean in JFM. Further analysis using data from 1982 to 2018, which covers both of the shorter time periods, yields results that are closer to those obtained using data from 2000 to 2018, with weaker negative correlations and limited areas over the Arctic Ocean.

In addition, the analysis explores the correlation of cloud amount and CRF in ON, NDJ, and JFM with the SO SIC index over EsCB and BKL using different starting years rather than 2000 and a fixed ending year of 2018. The results show that the negative correlations between JFM cloud amounts and CRF with the SO SIC index (which has the opposite sign of the SIC anomaly) over EsCB and BKL are significant, with confidence levels higher than 90%, for years starting at and after 1997 (Fig. A6). This suggests that the relationship between SO SIC over EsCB and BKL and JFM clouds underwent a change around 1997 or 1998, and the relationship holds with starting years at and after 1997.

The significant negative correlation between JFM cloud amounts and CRF and the SO SIC index over EsCB and BKL does not necessarily imply a causative relationship where the SO SIC changes directly cause changes in cloud amount and CRF over the Arctic Ocean in JFM. Other interannual forcings, such as SST and snow-cover anomalies, can influence atmospheric circulation and cloud properties as well (Simon et al. 2020). To investigate this further, the correlations between SST anomalies during SO and the SO SIC index over EsCB and BKL from 2000 to 2018 are calculated (Fig. 14). These correlations show negative values over the western coastal North American region, extending southward, and positive values over the central and northwest Pacific. This spatial pattern resembles the negative phase of the PDO (Mantua and Hare 2002; Mantua et al. 1997; Newman et al. 2016). Coincidentally, the PDO SO mean index also exhibits a transition from positive to negative around 1997 (Fig. A7). This may suggest that the relationship between JFM clouds and SO SIC could be modulated by the PDO forcing. To explore this hypothesis, lag corrections/regressions of cloud amount and CRF in ON, NDJ, and JFM on the SO PDO index from 2000 to 2018 are calculated. The results show that negative SO PDO precedes a general increase in cloud amount in ON, a general decrease in cloud amount in NDJ, and a decrease in cloud amount in JFM over the Arctic Ocean. However, none of these correlations and regressions are statistically significant. The statistically insignificant correlation/regression does not provide strong support for the PDO as the forcing mechanism that modulates both the SO SICs over EsCB and BKL and the cloud properties over the Arctic Ocean in JFM. A similar analysis using data from 1982 to 1999 also does not reveal any significant relationships between cloud amount and CRF in JFM and

(a) Correlation of SO SST on SO SIC index over EsCB

(b) Correlation of SO SST on SO SIC index over BKL

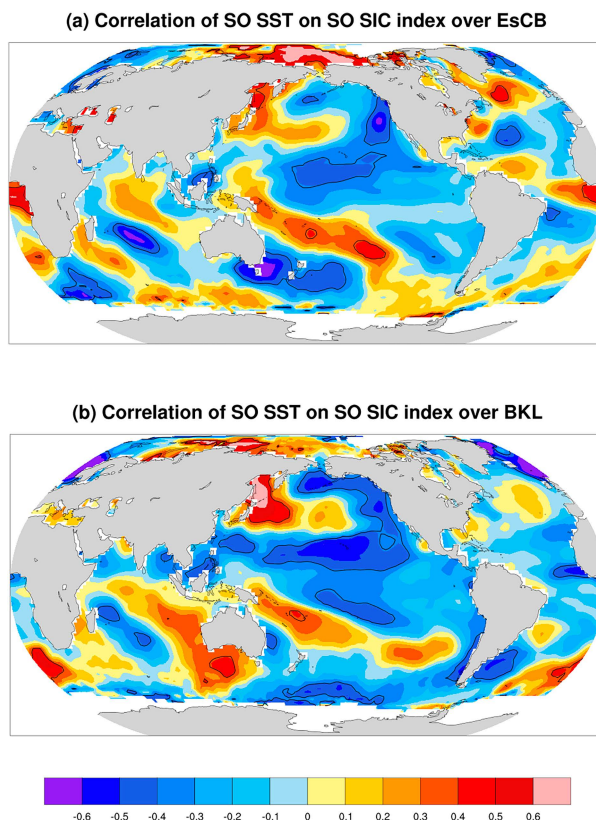-0.6 -0.5 -0.4 -0.3 -0.2 -0.1 0 0.1 0.2 0.3 0.4 0.5 0.6

FIG. 14. Correlation of the SST in SO and sea ice index in SO from 2000 to 2018 over (a) the EsCB and (b) the BKL. Contours of 90% confidence level of the correlations are shown as solid lines.

the SO PDO. Furthermore, no apparent pattern or significant correlation has been found between SO snow-cover anomalies and cloud property anomalies in JFM over the Arctic Ocean.

Previous studies have indeed demonstrated the important link between anomalous cloud amount and CRF in the wintertime over the Arctic Ocean and its impact on sea ice growth and the preconditioning of sea ice extent in the following summer. Thicker sea ice tends to melt more slowly, and ice motion can transport the thicker ice to other regions of the Arctic Ocean. Additionally, changes in summertime sea ice conditions have been shown to influence cloud properties due to factors such as increased surface evaporation, warmer surface temperatures, and altered lower-tropospheric structure. This study suggests that September and October sea ice changes are possibly associated with cloud amount and corresponding CRF from January to March. These changes in cloud amount and CRF, in turn, can influence sea ice growth and preconditioning for subsequent sea ice changes in September and October. The sign of the relationship between SO SIC changes and JFM cloud amount and CRF determines whether there could be a positive or negative cloud feedback on the SIC changes. For example, from 2000 to 2018, decreased SO SICs precede a decrease in cloud amount and CRF in JFM, leading to increased sea ice growth during this period. As a result, there is anomalously thicker sea ice over the Arctic Ocean in the following September

and October, indicating a negative feedback. Conversely, from 1982 to 1999, there may be a neutral or positive feedback, although the correlations between SO SIC changes and JFM cloud properties and CRF are not statistically significant.

Satellite cloud datasets from APP-x and CERES_EBAF_ Edition 4.1 were used in this study. Detecting clouds in polar regions using passive satellite sensors is challenging due to the similar temperatures and reflectances of low-level clouds and the surface. This task becomes even more difficult in winter, when reflectance data are unavailable, and temperature inversions are stronger (Liu et al. 2004, 2010). Since cloud detection is often the first step in satellite retrievals and the derived cloud mask is crucial for many other satellite products, Arctic cloud detection and cloud amount from passive satellite sensors have been extensively validated (Liu et al. 2010, 2012b, 2017) against observations from satellite-based and surface-based active sensors. It is worth noting that satellite cloud datasets have uncertainties due to resolution effect (Dutta et al. 2020), viewing angle effect (Maddux et al. 2010), diurnal cycle effect (Eastman and Warren 2014), data sampling effect (Liu 2015), and instrument sensitivity and methodology effect (Stubenrauch et al. 2012). Retrieving Arctic cloud properties such as cloud optical thickness, cloud effective radius, cloud water content, and radiative fluxes is equally if not more challenging for both passive and active satellite sensors because they rely on the quality of cloud detection and many other parameters (Key et al. 2016; Platnick et al. 2003; Liu et al. 2017). Ground-based cloud observations, including cloud water path from passive microwave radiometers in polar regions, are sparse and lack good spatial coverage. Cloud products from active sensors, like CloudSat and the Cloud–Aerosol Lidar and Infrared Pathfinder Satellite Observations (CALIPSO), do not have long enough records for use in this study (Liu et al. 2017).

5. Conclusions

The lag correlation and regression analysis conducted on cloud amount and cloud radiative forcing (CRF) over the Arctic Ocean and September–October (SO) sea ice concentration (SIC) changes over the East Siberian–Chukchi–Beaufort Seas (EsCB) and the Barents–Kara–Laptev Seas (BKL) reveals distinct relationships between the periods 2000–18 and 1982–99. From 2000 to 2018, a decrease in SO SIC over EsCB and BKL is associated with an overall increase in cloud amount during the subsequent October–November (ON), a decrease in cloud amount during November–January (NDJ), and a significant decrease in cloud amount during January–March (JFM) over the Arctic Ocean. The reduced cloud amount and negative CRF at the surface during JFM facilitate greater ice growth, preconditioning the sea ice and contributing to a more extensive sea ice extent and thicker sea ice the following September and October. This may suggest a negative cloud feedback on Arctic sea ice changes. Without this feedback, Arctic sea ice would have experienced more significant retreat during the period from 2000 to 2018.

In contrast, from 1982 to 1999, a decrease in SO SIC over EsCB leads to a general increase in cloud amount during NDJ and an increase in cloud amount during JFM over the Arctic Ocean. The increased cloud amount and positive CRF at the surface during JFM result in less ice growth, preconditioning the sea ice to be less extensive and thinner the following September and October. This may suggest a positive cloud feedback on summertime Arctic sea ice extent. This feedback contributed to faster sea ice retreat during the period from 1982 to 1999. These findings highlight the complex interactions between cloud properties, CRF, and sea ice changes in the Arctic.

The changes in JFM large-scale circulations and JFM temperature-dependent cloud microphysical processes associated with SO SIC anomalies may help explain the JFM cloud responses from 2000 to 2018 or 1982 to 1999. However, questions remain on how the SO SIC changes lead to the changes in those parameters/processes in JFM in the Arctic. One possible pathway is that the information on SIC changes in the summer and autumn is retained in the sea ice or underlying ocean into the following winter because of the much longer memory of sea ice and ocean than that of atmosphere. This stored information can have impacts both locally and over the Arctic Ocean through sea ice drift. Another possible pathway is that the SIC changes in EsCB and BKL lead to changes in large-scale circulation patterns. For example, Barents–Kara sea ice (BKS) loss in autumn triggers a negative North Atlantic Oscillation (NAO) the following winter, influencing the moisture transport into the Arctic Ocean (Strommen and Cooper 2024 and its cited references, Gimeno et al. 2019) and cloud formation (Liu et al. 2018). The different relationship between JFM clouds and SO SIC between 1982–99 and 2000–18 could be influenced by the transition of SO PDO from positive to negative around 1997. Further investigation in this study suggests that the time of switch between the different roles of clouds may have occurred around 1997, coinciding with the transition of the SO mean PDO index from generally positive to negative, and the correlation between SO SST and SICs from 2000 to 2018 also exhibits a pattern like that of the PDO. Although the lag correction and regression analysis of cloud amount and CRF over the Arctic Ocean and SO PDO shows similar patterns to the JFM cloud and SO SIC relationship, these correlations are not statistically significant. Therefore, the potential role of the PDO in modulating the cloud feedback on sea ice changes requires further investigation. Overall, the exact mechanisms and underlying factors connecting the SO sea ice changes and JFM cloud responses and driving the different responses of JFM Arctic clouds to SO sea ice changes are complex and require more comprehensive research to fully understand.

It is important to note that this paper does not reveal the physical mechanisms linking the SO SIC anomalies and wintertime cloud anomalies. Consequently, it does not explain how the sea ice changes lead to the varying responses of JFM Arctic clouds to SO SIC changes between the periods of 2000–18 and 1982–99. Further research is needed to uncover these mechanisms, which may confirm that the JFM Arctic clouds' response is driven by SO SIC changes or that both are influenced by another process.

Office. The authors thank Dr. Steve Vavrus of Center for Climatic Research of University of Wisconsin at Madison for his valuable suggestions on the work. The authors thank Dr. Daniel Vimont and Dr. Hannah Zanowski of University of Wisconsin at Madison for their help on statistical analysis. The views, opinions, and findings contained in this report are those of the author and should not be construed as an official National Oceanic and Atmospheric Administration or U.S. Government position, policy, or decision.

Data availability statement. All datasets used in this study are publicly available. The extended AVHRR Polar Pathfinder (APP-x) climate data record are available at https://www.ncei. noaa.gov/access/metadata/landing-page/bin/iso?id=gov.noaa. ncdc:C00941. The CERES Energy Balance and Filled (EBAF) data are available at https://ceres.larc.nasa.gov/data/. The Extended Reconstructed Sea Surface Temperature (ERSST) dataset is available at https://www.ncei.noaa.gov/pub/data/cmb/ ersst/v5/netcdf/. The ERA5 monthly mean data are available at https://cds.climate.copernicus.eu/datasets/reanalysis-era5-pressure-levels-monthly-means?tab=download. The sea ice concentration data and snow cover data are from the National Snow and Ice Data Center at https://nsidc.org/data/g02202/versions/4 and https://nsidc.org/data/g10035/versions/1. The National Centers for Environmental Information (NCEI) Pacific decadal oscillation (PDO) index data are available at https://www.ncei.noaa. gov/pub/data/cmb/ersst/v5/index.ersst.v5.pdo.dat.

APPENDIX

Appendix of Auxiliary Figures

Appendix includes some figures that are referred to in the manuscript (Figs. A1–A7).
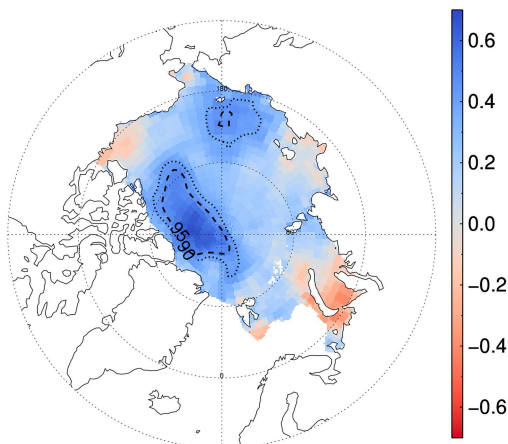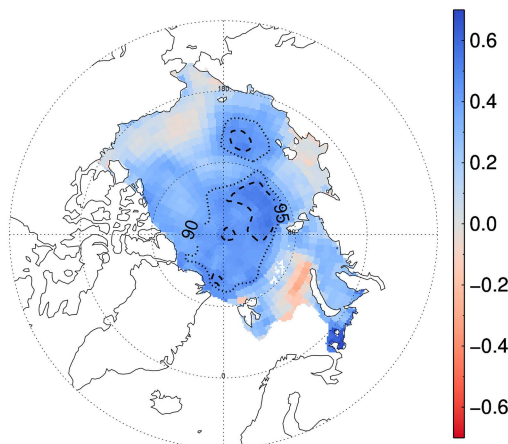
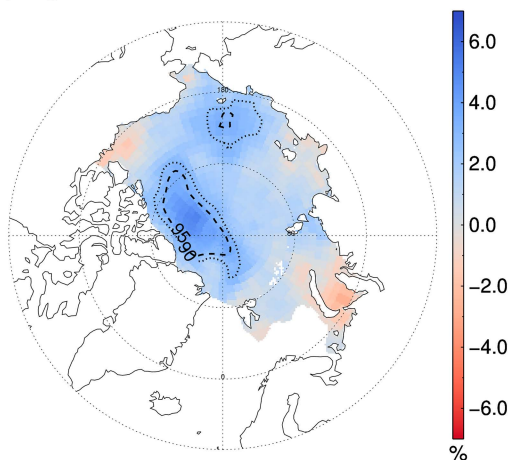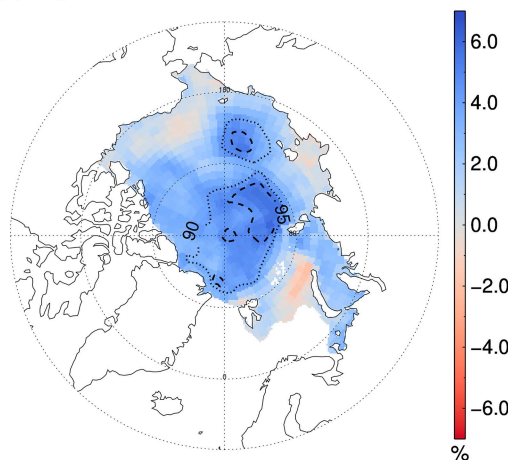FIG. A1. Correlations of the CERES cloud amount (cmask) in JFM and the sea ice index in SO from 2000 to 2018 over (a) the EsCB and (b) the BKL. The regression of the CERES cloud amount (cmask) in JFM onto the sea ice index in SO from 2000 to 2018 over is shown in (c) EsCB and (d) BKL. The dotted-line and dashed-line contours denote that correlations/regressions within have higher than 90% and 95% confidence levels, respectively. The solid-line contours denote the areas with *p* values smaller than the false discovery rate probability, meaning that they pass the FST.
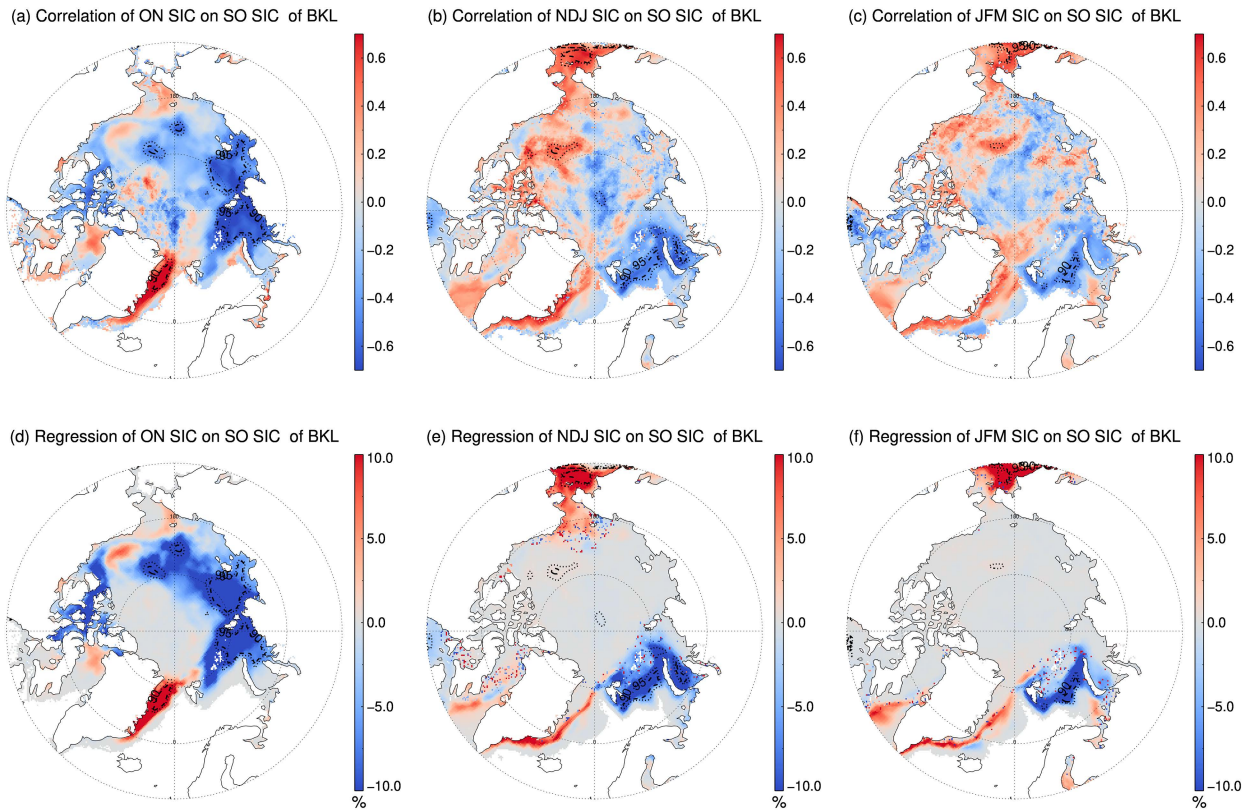
FIG. A2. Correlation of the SIC anomalies in (a) ON, (b) NDJ, and (c) JFM with sea ice index in SO for the period 2000–18 over the BKL Seas. The lag regression coefficients of the SIC anomalies on the SO sea ice index.
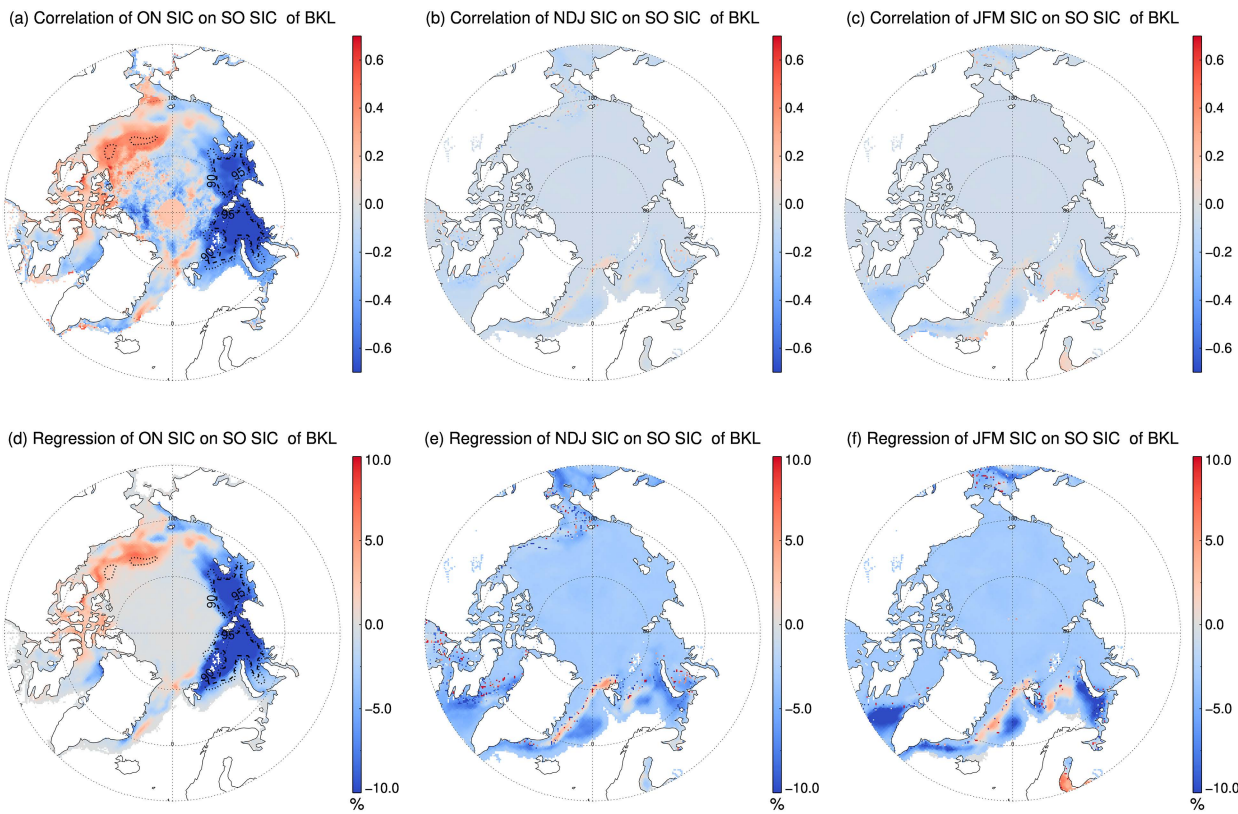
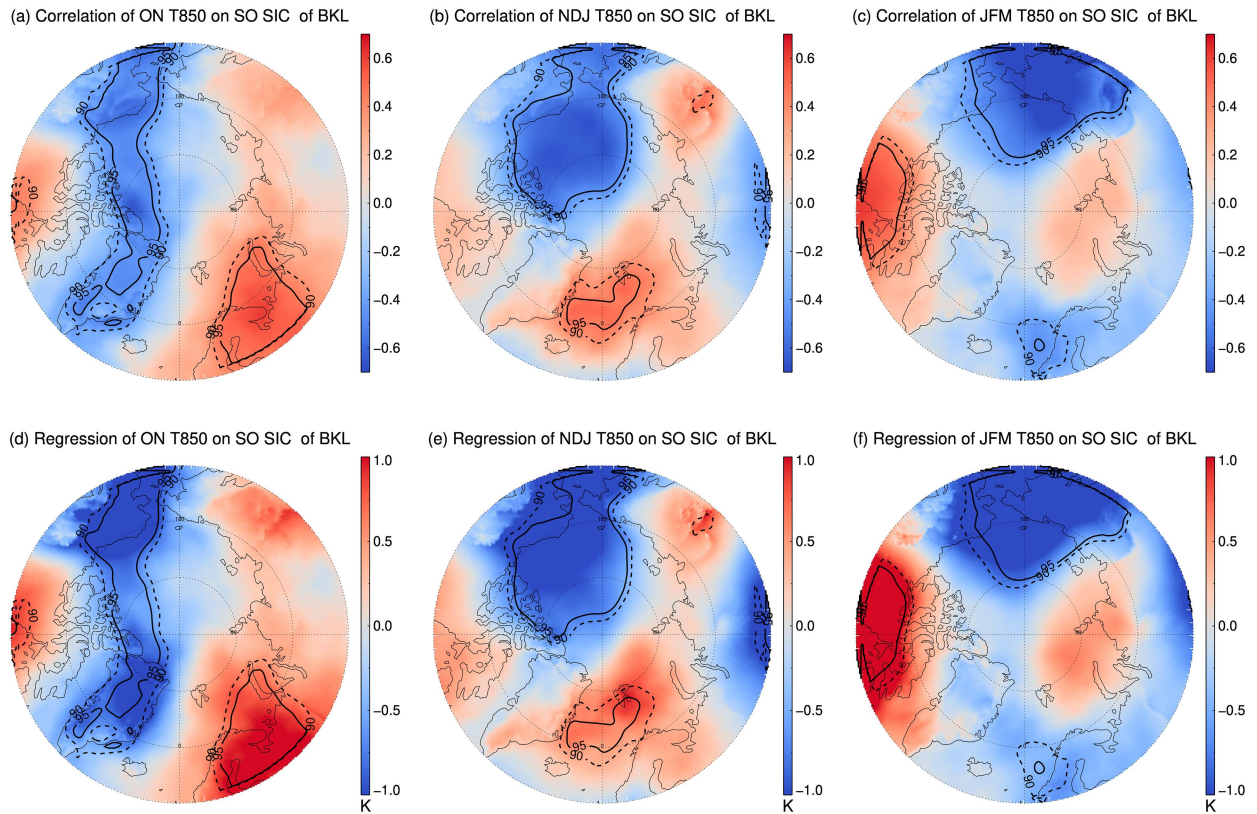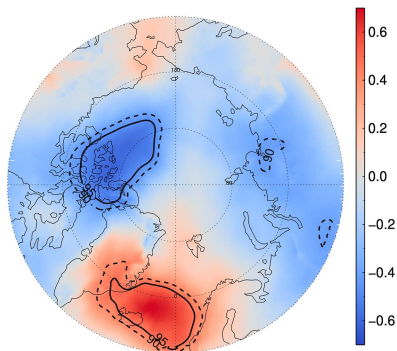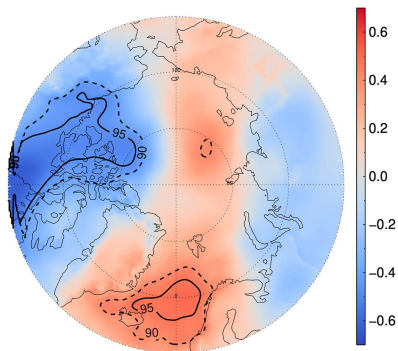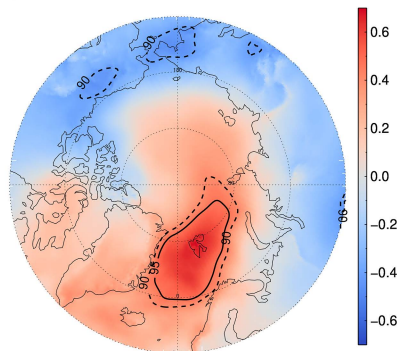FIG. A3. As in Fig. A2, but for 1982–99.

FIG. A4. Correlation of the ERA5 850-hPa temperature anomalies (T850) in (a) ON, (b) NDJ, and (c) JFM with sea ice index in SO for the period 2000–18 over the EsCB. The lag regression coefficients of the 850-hPa temperature anomalies (T850) on the SO sea ice index.
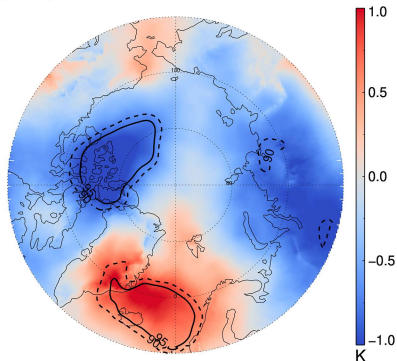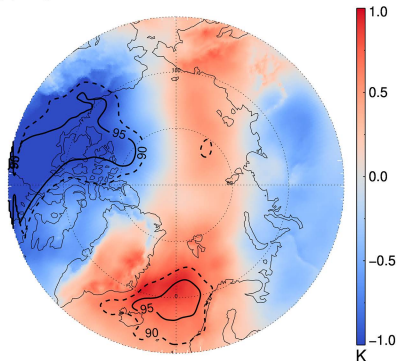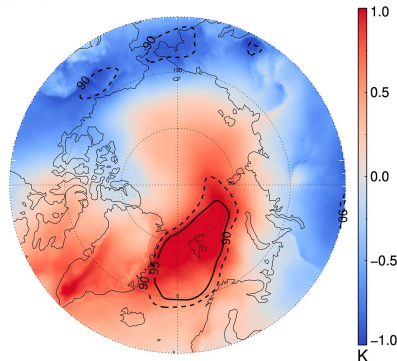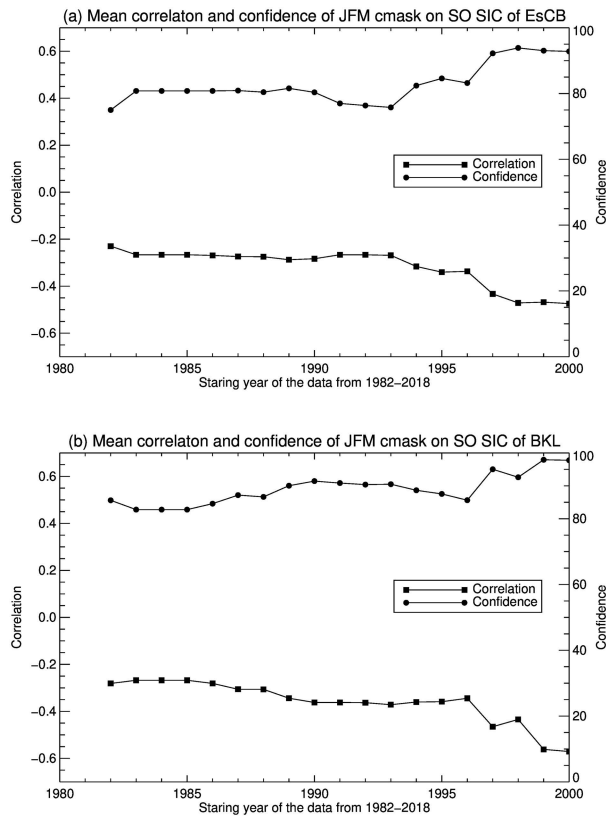
FIG. A5. As in Fig. A4, but for 1982–99.

FIG. A6. The mean correlation and confidence level over the area 70°–90°N, 90°–210°E between the JFM cloud amounts (cmask) and SO SIC index over (top) EsCB and (bottom) BKL using data with a ending year of 2018 and starting year varying from 1982 to 2000.
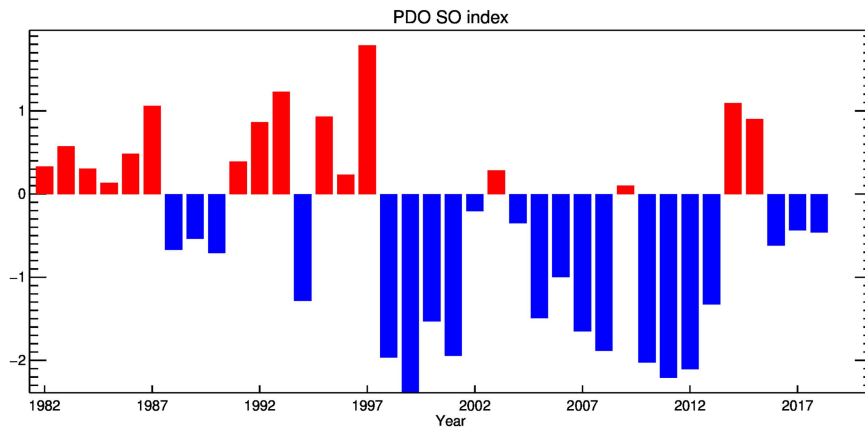

FIG. A7. PDO SO mean time series.

REFERENCES

Arias, P. A., and Coauthors, 2023: Technical summary. *Climate Change 2021: The Physical Science Basis*, V. Masson-Delmotte et al., Eds., Cambridge University Press, 35–144, https://doi.org/10.1017/9781009157896.002.

Beesley, J. A., and R. E. Moritz, 1999: Toward an explanation of the annual cycle of cloudiness over the Arctic Ocean. *J. Climate*, **12**, 395–415, https://doi.org/10.1175/1520-0442(1999)012<0395:TAEOTA>2.0.CO;2.

Curry, J. A., J. L. Schramm, W. B. Rossow, and D. Randall, 1996: Overview of Arctic cloud and radiation characteristics. *J. Climate*, **9**, 1731–1764, https://doi.org/10.1175/1520-0442(1996)009<1731:OOACAR>2.0.CO;2.

Ding, S., B. Wu, and W. Chen, 2021: Dominant characteristics of early autumn Arctic sea ice variability and its impact on winter Eurasian climate. *J. Climate*, **34**, 1825–1846, https://doi.org/10.1175/JCLI-D-19-0834.1.

Dutta, S., L. Di Girolamo, S. Dey, Y. Zhan, C. M. Moroney, and G. Zhao, 2020: The reduction in near-global cloud cover after correcting for biases caused by finite resolution measurements. *Geophys. Res. Lett.*, **47**, e2020GL090313, https://doi.org/10.1029/2020GL090313.

Eastman, R., and S. G. Warren, 2014: Diurnal cycles of cumulus, cumulonimbus, stratus, stratocumulus, and fog from surface observations over land and ocean. *J. Climate*, **27**, 2386–2404, https://doi.org/10.1175/JCLI-D-13-00352.1.

Eisenman, I., N. Untersteiner, and J. S. Wettlaufer, 2007: On the reliability of simulated Arctic sea ice in global climate models. *Geophys. Res. Lett.*, **34**, L10501, https://doi.org/10.1029/2007GL029914.

Fučkar, N. S., V. Guemas, N. C. Johnson, F. Massonnet, and F. J. Doblas-Reyes, 2016: Clusters of interannual sea ice variability in the northern hemisphere. *Climate Dyn.*, **47**, 1527–1543, https://doi.org/10.1007/s00382-015-2917-2.

Gimeno, L., M. Vázquez, J. Eiras-Barca, R. Sorí, I. Algarra, and R. Nieto, 2019: Atmospheric moisture transport and the decline in Arctic Sea ice. *Wiley Interdiscip. Rev.: Climate Change*, **10**, e588, https://doi.org/10.1002/wcc.588.

Hersbach, H., and Coauthors, 2020: The ERA5 global reanalysis. *Quart. J. Roy. Meteor. Soc.*, **146**, 1999–2049, https://doi.org/10.1002/qj.3803.

Huang, B., and Coauthors, 2020: Uncertainty estimates for sea surface temperature and land surface air temperature in NOAAGlobalTemp version 5. *J. Climate*, **33**, 1351–1379, https://doi.org/10.1175/JCLI-D-19-0395.1.

Huang, Y., Q. Ding, X. Dong, B. Xi, and I. Baxter, 2021: Summertime low clouds mediate the impact of the large-scale circulation on Arctic sea ice. *Commun. Earth Environ.*, **2**, 38, https://doi.org/10.1038/s43247-021-00114-w.

Intrieri, J. M., C. W. Fairall, M. D. Shupe, P. O. G. Persson, E. L. Andreas, P. S. Guest, and R. E. Moritz, 2002: An annual cycle of Arctic surface cloud forcing at SHEBA. *J. Geophys. Res.*, **107**, 8039, https://doi.org/10.1029/2000JC000439.

Kapsch, M.-L., R. G. Graversen, and M. Tjernström, 2013: Springtime atmospheric energy transport and the control of Arctic summer sea-ice extent. *Nat. Climate Change*, **3**, 744–748, https://doi.org/10.1038/nclimate1884.

Kato, S., and Coauthors, 2020: Uncertainty in satellite-derived surface irradiances and challenges in producing surface radiation budget climate data record. *Remote Sens.*, **12**, 1950, https://doi.org/10.3390/rs12121950.

Kay, J. E., and A. Gettelman, 2009: Cloud influence on and response to seasonal Arctic sea ice loss. *J. Geophys. Res.*, **114**, D18204, https://doi.org/10.1029/2009JD011773.

Key, J., and X. Wang, 2015: Climate Algorithm Theoretical Basis Document for the extended AVHRR Polar Pathfinder (APP-x). Tech Rep. CDRP ATBD 0573, revision 1.0, 83 pp., https://pubs.ssec.wisc.edu/research_Resources/publications/pdfs/SSECPUBS/SSEC_Publication_No_15_09_K1.pdf.

——, ——, Y. Liu, R. Dworak, and A. Letterly, 2016: The AVHRR polar pathfinder climate data records. *Remote Sens.*, **8**, 167, https://doi.org/10.3390/rs8030167.

Kwok, R., 2018: Arctic sea ice thickness, volume, and multiyear ice coverage: Losses and coupled variability (1958–2018). *Environ. Res. Lett.*, **13**, 105005, https://doi.org/10.1088/1748-9326/aae3ec.

Letterly, A., J. Key, and Y. Liu, 2016: The influence of winter cloud on summer sea ice in the Arctic, 1983–2013. *J. Geophys. Res. Atmos.*, **121**, 2178–2187, https://doi.org/10.1002/2015JD024316.

Li, X., S. K. Krueger, C. Strong, G. G. Mace, and S. Benson, 2020: Midwinter Arctic leads form and dissipate low clouds. *Nat. Commun.*, **11**, 206, https://doi.org/10.1038/s41467-019-14074-5.

Liu, Y., 2015: Estimating errors in cloud amount and cloud optical thickness due to limited spatial sampling using a satellite imager as a proxy for nadir-view sensors. *J. Geophys. Res. Atmos.*, **120**, 6980–6991, https://doi.org/10.1002/2015JD023507.

——, and J. R. Key, 2014: Less winter cloud aids summer 2013 Arctic sea ice return from 2012 minimum. *Environ. Res. Lett.*, **9**, 044002, https://doi.org/10.1088/1748-9326/9/4/044002.

——, ——, R. A. Frey, S. A. Ackerman, and W. P. Menzel, 2004: Nighttime polar cloud detection with MODIS. *Remote Sens. Environ.*, **92**, 181–194, https://doi.org/10.1016/j.rse.2004.06.004.

——, ——, J. A. Francis, and X. Wang, 2007: Possible causes of decreasing cloud cover in the Arctic winter, 1982–2000. *Geophys. Res. Lett.*, **34**, L14705, https://doi.org/10.1029/2007GL030042.

——, S. A. Ackerman, B. C. Maddux, J. R. Key, and R. A. Frey, 2010: Errors in cloud detection over the Arctic using a satellite imager and implications for observing feedback mechanisms. *J. Climate*, **23**, 1894–1907, https://doi.org/10.1175/2009JCLI3386.1.

——, J. R. Key, Z. Liu, X. Wang, and S. J. Vavrus, 2012a: A cloudier Arctic expected with diminishing sea ice. *Geophys. Res. Lett.*, **39**, L05705, https://doi.org/10.1029/2012GL051251.

——, ——, S. A. Ackerman, G. G. Mace, and Q. Zhang, 2012b: Arctic cloud macrophysical characteristics from CloudSat and CALIPSO. *Remote Sens. Environ.*, **124**, 159–173, https://doi.org/10.1016/j.rse.2012.05.006.

——, M. D. Shupe, Z. Wang, and G. Mace, 2017: Cloud vertical distribution from combined surface and space radar–Lidar observations at two Arctic atmospheric observatories. *Atmos. Chem. Phys.*, **17**, 5973–5989, https://doi.org/10.5194/acp-17-5973-2017.

——, J. R. Key, S. Vavrus, and C. Woods, 2018: Time evolution of the cloud response to moisture intrusions into the Arctic during winter. *J. Climate*, **31**, 9389–9405, https://doi.org/10.1175/JCLI-D-17-0896.1.

——, ——, X. Wang, and M. Tschudi, 2020: Multidecadal Arctic sea ice thickness and volume derived from ice age. *Cryosphere*, **14**, 1325–1345, https://doi.org/10.5194/tc-14-1325-2020.

Livezey, R. E., and W. Y. Chen, 1983: Statistical field significance and its determination by Monte Carlo techniques. *Mon. Wea.*

Rev., **111**, 46–59, https://doi.org/10.1175/1520-0493(1983)111<0046:SFSAID>2.0.CO;2.

Maddux, B. C., S. A. Ackerman, and S. Platnick, 2010: Viewing geometry dependencies in MODIS cloud products. *J. Atmos. Oceanic Technol.*, **27**, 1519–1528, https://doi.org/10.1175/2010JTECHA1432.1.

Mantua, N. J., and S. R. Hare, 2002: The Pacific decadal oscillation. *J. Oceanogr.*, **58**, 35–44, https://doi.org/10.1023/A:1015820616384.

——, ——, Y. Zhang, J. M. Wallace, and R. C. Francis, 1997: A Pacific interdecadal climate oscillation with impacts on salmon production. *Bull. Amer. Meteor. Soc.*, **78**, 1069–1080, https://doi.org/10.1175/1520-0477(1997)078<1069:APICOW>2.0.CO;2.

Meier, W. N., and J. Stroeve, 2022: An updated assessment of the changing Arctic sea ice cover. *Oceanography*, **35** (3–4), 10–19, https://doi.org/10.5670/oceanog.2022.114.

——, F. Fetterer, A. K. Windnagel, and J. S. Stewart, 2021: NOAA/NSIDC climate data record of passive microwave sea ice concentration, version 4. Distributed by National Snow and Ice Data Center, accessed 11 January 2022, https://doi.org/10.7265/efmz-2t65.

Newman, M., and Coauthors, 2016: The Pacific decadal oscillation, revisited. *J. Climate*, **29**, 4399–4427, https://doi.org/10.1175/JCLI-D-15-0508.1.

Palm, S. P., S. T. Strey, J. Spinhirne, and T. Markus, 2010: Influence of Arctic sea ice extent on polar cloud fraction and vertical structure and implications for regional climate. *J. Geophys. Res.*, **115**, D21209, https://doi.org/10.1029/2010JD013900.

Platnick, S., M. D. King, S. A. Ackerman, W. P. Menzel, B. A. Baum, J. C. Riedi, and R. A. Frey, 2003: The MODIS cloud products: Algorithms and examples from terra. *IEEE Trans. Geosci. Remote Sens.*, **41**, 459–473, https://doi.org/10.1109/TGRS.2002.808301.

Renard, B., and Coauthors, 2008: Regional methods for trend detection: Assessing field significance and regional consistency. *Water Resour. Res.*, **44**, W08419, https://doi.org/10.1029/2007WR006268.

Robinson, D. A., and T. W. Estilow, 2021: Rutgers Northern Hemisphere 24 km weekly snow cover extent, September 1980 onward, version 1. National Snow and Ice Data Center, accessed 11 February 2022, https://doi.org/10.7265/zzbm-2w05.

Schweiger, A. J., R. W. Lindsay, S. Vavrus, and J. A. Francis, 2008: Relationships between Arctic sea ice and clouds during autumn. *J. Climate*, **21**, 4799–4810, https://doi.org/10.1175/2008JCLI2156.1.

Serreze, M. C., and R. G. Barry, 2005: *The Arctic Climate System*. Cambridge University Press, 385 pp.

Shupe, M. D., and J. M. Intrieri, 2004: Cloud radiative forcing of the Arctic surface: The influence of cloud properties, surface albedo, and solar zenith angle. *J. Climate*, **17**, 616–628, https://doi.org/10.1175/1520-0442(2004)017<0616:CRFOTA>2.0.CO;2.

Simon, A., C. Frankignoul, G. Gastineau, and Y.-O. Kwon, 2020: An observational estimate of the direct response of the cold-season atmospheric circulation to the Arctic sea ice loss. *J. Climate*, **33**, 3863–3882, https://doi.org/10.1175/JCLI-D-19-0687.1.

Strommen, K., and F. C. Cooper, 2024: Physical and unphysical causes of nonstationarity in the relationship between Barents-Kara sea ice and the North Atlantic Oscillation. *Geophys. Res. Lett.*, **51**, e2023GL107609, https://doi.org/10.1029/2023GL107609.

Stubenrauch, C. J., W. B. Rossow, and S. Kinne, 2012: Assessment of global cloud datasets from satellites: A project of the world climate research programme Global Energy and Water Cycle Experiment (GEWEX) radiation panel. WCRP Rep. 23/2012, 176 pp., https://www.wcrp-climate.org/documents/GEWEX_Cloud_Assessment_2012.pdf.

Tan, I., and T. Storelvmo, 2019: Evidence of strong contributions from mixed-phase clouds to Arctic climate change. *Geophys. Res. Lett.*, **46**, 2894–2902, https://doi.org/10.1029/2018GL081871.

Taylor, P. C., S. Kato, K.-M. Xu, and M. Cai, 2015: Covariance between Arctic sea ice and clouds within atmospheric state regimes at the satellite footprint level. *J. Geophys. Res. Atmos.*, **120**, 12 656–12 678, https://doi.org/10.1002/2015JD023520.

Thorndike, A. S., 1992: A toy model linking atmospheric thermal radiation and sea ice growth. *J. Geophys. Res.*, **97**, 9401–9410, https://doi.org/10.1029/92JC00695.

Trepte, Q. Z., and Coauthors, 2019: Global cloud detection for CERES edition 4 using terra and aqua MODIS data. *IEEE Trans. Geosci. Remote Sens.*, **57**, 9410–9449, https://doi.org/10.1109/TGRS.2019.2926620.

Tschudi, M. A., W. N. Meier, and J. S. Stewart, 2020: An enhancement to sea ice motion and age products at the National Snow and Ice Data Center (NSIDC). *Cryosphere*, **14**, 1519–1536, https://doi.org/10.5194/tc-14-1519-2020.

Wang, Y., X. Yuan, H. Bi, Y. Liang, H. Huang, Z. Zhang, and Y. Liu, 2019: The contributions of winter cloud anomalies in 2011 to the summer sea-ice rebound in 2012 in the Antarctic. *J. Geophys. Res. Atmos.*, **124**, 3435–3447, https://doi.org/10.1029/2018JD029435.

Wilks, D. S., 2016: "The stippling shows statistically significant grid points": How research results are routinely overstated and overinterpreted, and what to do about it. *Bull. Amer. Meteor. Soc.*, **97**, 2263–2273, https://doi.org/10.1175/BAMS-D-15-00267.1.